Chapter 7

Wake Structures and Aerodynamic Performance of Flapping Airfoils

In the previous chapters, we reviewed the aerodynamics of low Reynolds number flapping flight, where we covered topics such as dynamic stall, vortex shedding, thrust generation due to flapping flight, flapping flight in terms of Reynolds number, Strouhal number and reduced frequency, and flapping flight performance and kinematics. We also presented the method of overlapping grids used to efficiently tackle the problem of moving/deforming bodies and the numerical method used to solve the governing equations on overlapping grids. In this chapter, we present several two dimensional results for heaving and coupled heaving-and-pitching motions. The interest here is to determine the values of flapping frequency and flapping amplitude best suited for flapping flight, in terms of maximum efficiency and thrust production. We also study the influence of airfoil cambering and airfoil flexibility on lift and thrust generation.

7.1 Introduction

As discussed in Chapter 2, Section 2.3, the aerodynamic forces on a body are related to the wake produced by the body. The flow over a stationary airfoil or over an airfoil flapping at a specific frequency and amplitude is constituted by a von Karman vortex street, consisting of alternating rows of clockwise (top) and counter-clockwise (bottom) rotating vortices (see figure 7.1). The time-averaged velocity profile produced by such a configuration is a momentum deficit profile, in that the mean velocity in the wake is lower than the free-stream value. Vortex pairs form mushroom-like structures which are tilted upstream (see figure 7.1). The velocity profile and the upstream-tilted vortex structures are signatures that the body is producing drag.

If the rows of vortices are exchanged so that we have counterclockwise (top) and clockwise (bottom) rotating vortex rows, the configuration is known as a reverse Karman vortex street. The resulting time-averaged velocity profile is now a momentum surfeit (jet) profile, such that the mean velocity is higher than the free-stream. The vortex pairs now form mushroom-like structures that are tilted downstream (see figure 7.2). The momentum surfeit velocity profile and the downstream-tilted vortex structures indicate that the body is producing net thrust.

At the point where thrust due to flapping and the airfoil drag exactly balance, we might expect to see a neutral wake, where the vortices are collinear and mushroom-like vortex pairs are not

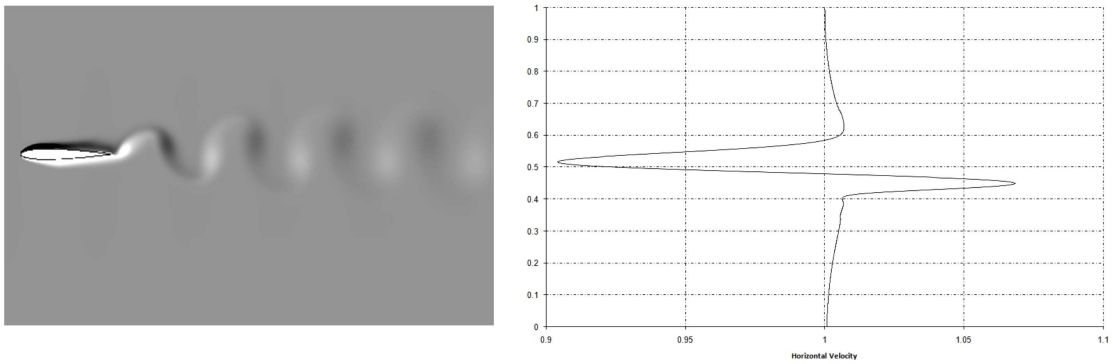

Figure 7.1: *Left: wake structure behind a heaving NACA 0012 airfoil (vorticity contours). Right: horizontal velocity profile measured at a distance equal to 5 times the airfoil chord away from the trailing edge. Flapping parameters:* $St = 0.1, h_a = 0.05, Re = 1100$. *This configuration is indicative of drag production.*

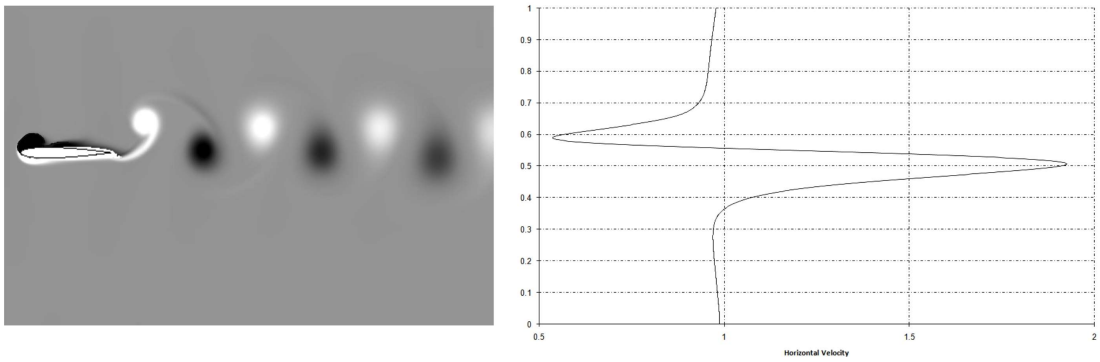

Figure 7.2: *Left: wake structure behind a heaving NACA 0012 airfoil (vorticity contours). Right: horizontal velocity profile measured at a distance equal to 5 times the airfoil chord away from the trailing edge. Flapping parameters:* $St = 0.3, h_a = 0.15, Re = 1100$. *This configuration is indicative of thrust production.*

tilted, as shown in figure 7.3.

Taylor *et al.* [182] performed a study of published wing beat frequencies and amplitudes and cruise speeds, across a range of birds, bats and insects, to determine Strouhal numbers in cruising flight. They found 75% of the 42 species considered to fall within a narrow range of $0.19 < St < 0.41$, with a mean value of $St = 0.29$. Triantafyllou *et al.* [193], provided a graph of measured Strouhal numbers for a range of fishes, sharks and cetaceans, with all falling largely within the Strouhal number range of $0.25 < St < 0.35$. In the results presented by Nudds *et al.* [136], they found that their calculations were consistent with the hypothesis that birds have converged upon a narrow optimum range of St in cruising flight. The best estimates of St for the empirical data given by them fell within the range of $0.2 < St < 0.4$ associated with high propulsive efficiency in other theoretical and experimental studies [152, 193].

Hereafter, we study the dependency of the wake structure and aerodynamic performance on the flapping and geometric parameters such as, flapping frequency, flapping amplitude and airfoil

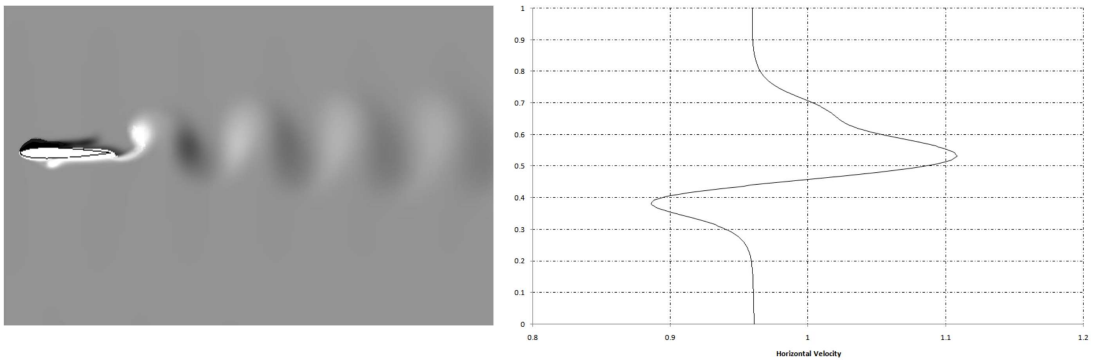

Figure 7.3: *Left: wake structure behind a heaving NACA 0012 airfoil (vorticity contours). Right: horizontal velocity profile measured at a distance equal to 5 times the airfoil chord away from the trailing edge. Flapping parameters:* $St = 0.15, h_a = 0.25, Re = 1100$. *This configuration is indicative of a net balance between thrust production and drag generation (neutral wake).*

geometry (between others), for airfoils undergoing pure heaving motion or coupled heaving-and-pitching motion (flapping motion).

7.2 Heaving Airfoil Wake Signature and Aerodynamic Performance

In order to characterize the wake signature of a heaving airfoil and its dependency on the flapping parameters, we conduct an extensive numerical experiment, where we simulate a NACA 0012 airfoil, undergoing heaving motion as per equation 2.21. The Reynolds number based on the airfoil chord was chosen to be equal to $Re = 1100$. In table 7.1 we present the flapping parameters for this numerical experiment.

Airfoil type	Re	St	h_a	f_h
NACA 0012	1100	$0.1 < St < 1.4$	$0.05 < h_a < 1$	$0.025 < f_h < 10$

Table 7.1: *Flapping parameters for the pure heaving case.*

But before discussing the results of the parametric study, let us first take a look at the heaving motion (eq. 2.21) and at the evolution of lift and thrust coefficients with time for a single case. In figure 7.4 the heaving kinematics is plotted, where one period consists of an up and down stroke. Since the airfoil is symmetric and is oscillating symmetrically about the mean horizontal line, we expect a symmetrical lift evolution (but this does not necessary hold for certain values of h_a and f_h, as presented later). The bumps appearing in the lift coefficient curve corresponds to the dynamics of the leading edge vortex, which will be studied in a later section. The frequency of the thrust coefficient is twice that of the lift coefficient because thrust is generated in both the up and down strokes.

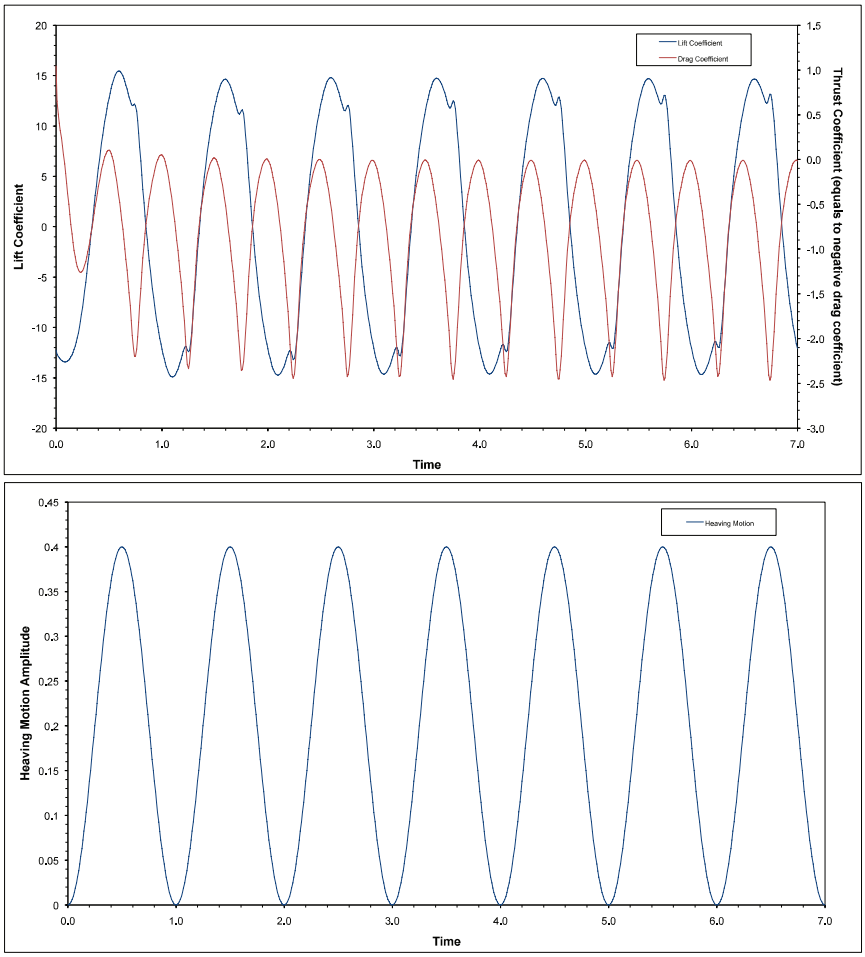

Figure 7.4: *Top figure: time dependent drag and lift coefficients (where negative values of drag coefficient indicate thrust production). Bottom figure: heaving kinematics. Flapping parameters:* $Re = 1100, St = 0.4, h_a = 0.2$ ($\overline{c_t} = 0.8834$, $\overline{c_l} = 0.0098$).

In figure 7.5, we plot the values of average thrust coefficient $\overline{c_t}$ and propulsion efficiency η obtained for Strouhal number values ranging from $0.1 < St < 0.7$, at a fixed heaving frequency $f_h = 1\,(k = 3.14159)$. In this figure, we can clearly identify three regimes: 1) one corresponding to drag production for Strouhal number values approximately $St < 0.18$, 2) a second regime for Strouhal values between $0.18 < St < 0.2$, corresponding to a very narrow transition area where no or very little thrust (or drag) is produced, and 3) a final regime corresponding to thrust generation for Strouhal number values $St > 0.2$, with a maximum propulsive efficiency value obtained at $St = 0.3$.

In the results shown in figure 7.5, the Strouhal number was varied by adjusting the heaving amplitude h_a. But our parameter space (f_h, h_a) is not only limited to one fixed value of f_h, both h_a and f_h can be changed independently, hence, our test matrix becomes quite large. Clearly, the previous experiment does not cover the whole parameter space, but it is a good indicator as far as wake signature characterization is concerned; a more extensive parameter search is however

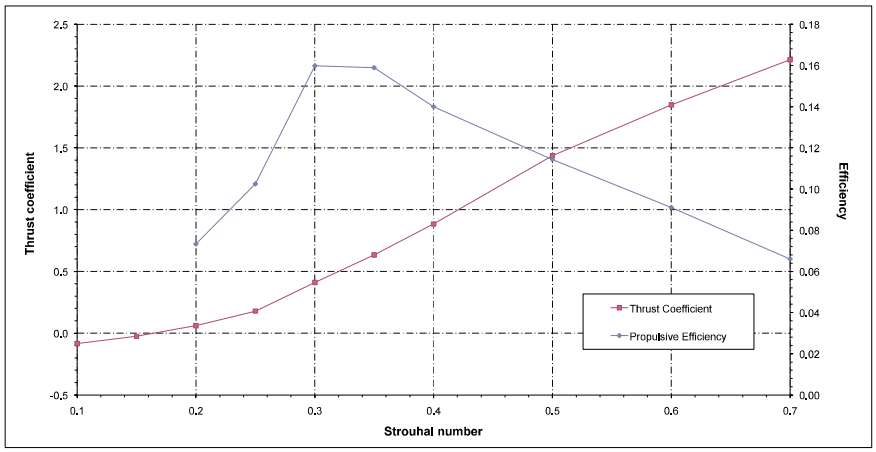

Figure 7.5: *Variation of thrust coefficient and propulsive efficiency with the Strouhal number. Flapping parameters:* $Re = 1100, f_h = 1$. *Notice that the propulsive efficiency is only shown for positive thrust.*

necessary to identify the regime(s) with the largest efficiency.

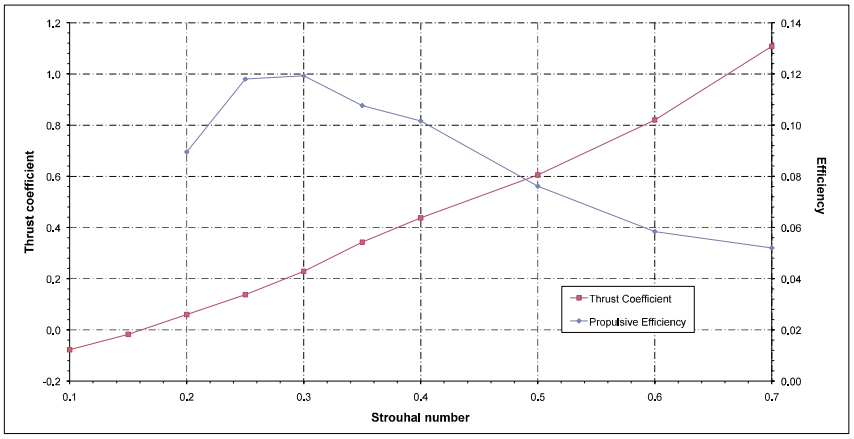

Figure 7.6: *Variation of thrust coefficient and propulsive efficiency with the Strouhal number. Flapping parameters:* $Re = 1100, f_h = 0.5$. *Notice that the propulsive efficiency is only shown for positive thrust.*

For purposes of comparison, in figure 7.6, we illustrate a similar plot where the heaving frequency is fixed to $f_h = 0.5\,(k = 1.570795)$ and the Strouhal number varies between $0.1 < St < 0.7$. Again, the maximum efficiency is obtained at $St = 0.3$. In this figure, the drag production regime approximately corresponds to $St < 0.15$ and the thrust production regime to $St > 0.2$, with a very narrow transition area between $0.15 < St < 0.20$, where no or little thrust (or drag) is produced. As it can be evidenced from figures 7.5 and 7.6, the heaving frequency have also a direct influence on whether the airfoil produces thrust or drag and hence on the wake topology.

Let us now fix the Strouhal number value to $St = 0.3$ (corresponding to the maximum efficiency value in figure 7.5) and vary the values of the heaving amplitude h_a and heaving frequency f_h, as

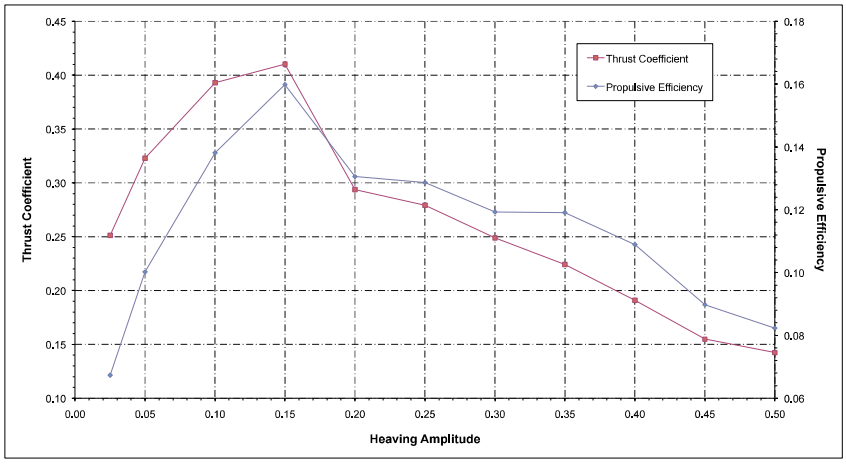

Figure 7.7: *Variation of thrust coefficient and propulsive efficiency with heaving amplitude. Flapping parameters:* $Re = 1100, St = 0.3$.

shown in figure 7.7. In this figure, the maximum efficiency value corresponds to a heaving amplitude value of $h_a = 0.15$ (same value as the case shown in figure 7.5). But this is not necessarily the same for other configurations in parameter space (f_h, h_a), as shown in figure 7.8, where we fix the Strouhal number $St = 0.4$ (thrust production regime) and we change the values of the heaving amplitude h_a and the heaving frequency f_h accordingly. Here, the maximum propulsive efficiency value corresponds to a heaving amplitude value $h_a = 0.30$ and a heaving frequency value $f_h = 0.666667$ ($k \approx 2.094$), which are not the same values for the case presented in figure 7.5.

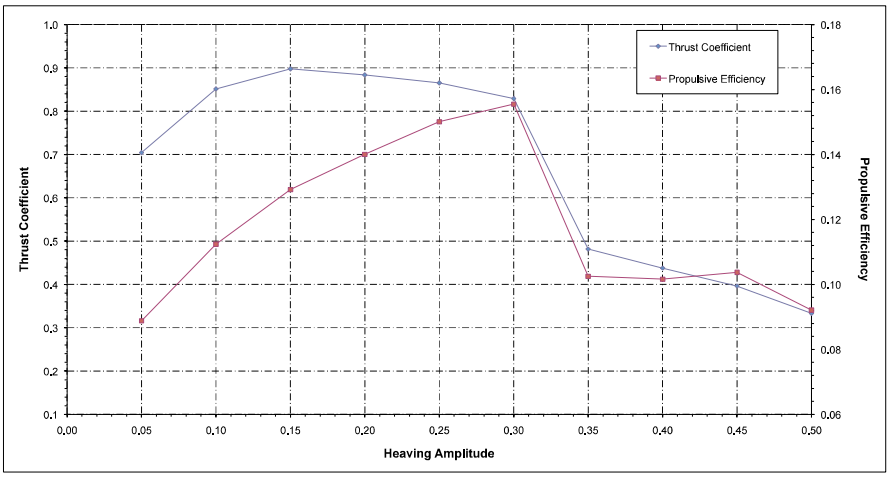

Figure 7.8: *Variation of thrust coefficient and propulsive efficiency with heaving amplitude. Flapping parameters:* $Re = 1100, St = 0.4$.

From the above discussion, we can conclude that the Strouhal number (based on the trailing edge excursion or heaving amplitude h_a) seems to be enough for wake signature characterization, but is not sufficient insofar as maximum efficiency is concerned. Both heaving amplitude h_a and

heaving frequency f_h (hence the Strouhal number St and the reduced frequency k), should be adjusted separately.

In figure 7.9, the previous results are extended as to characterize the wake topology for a wider range of heaving amplitude and heaving frequency combinations, the plot obtained is similar to that used by Triantafyllou *et al.* [191], Jones *et al.* [97] and Lua *et al.* [115]. In this figure, the numerically simulated wakes are classified according to the observed vortex positions. Lines of constant St are included demonstrating the approximate dependence of the numerical results on the Strouhal number. The wakes are classified as drag producing, neutral, thrust producing, deflected wake and jet-switching wake.

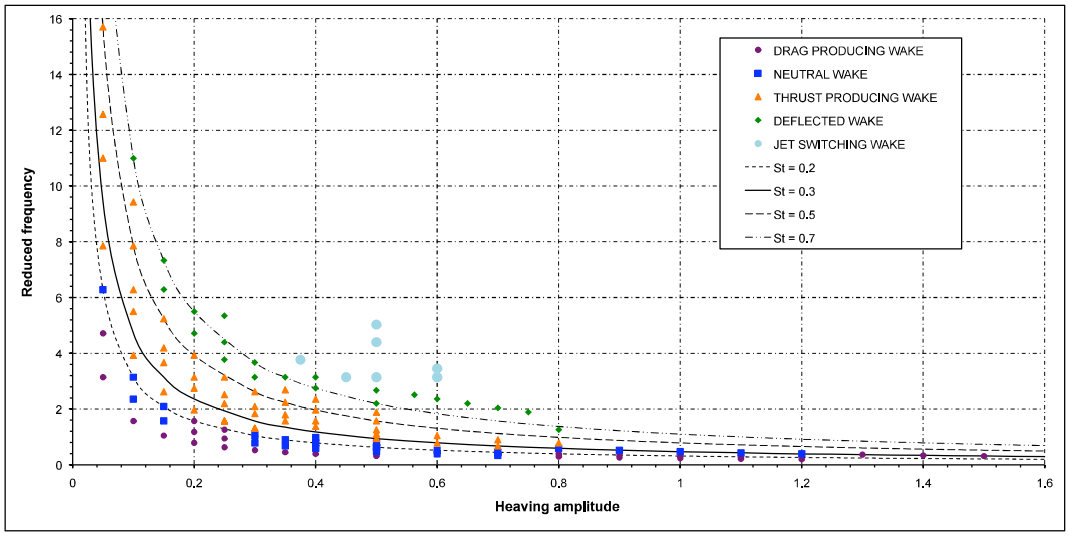

Figure 7.9: *Plot showing the wake structure classification. Lines of constant Strouhal number value are included to demonstrate the approximate dependence of the wake topology on the Strouhal number.*

In figure 7.9, it is observed that for low values of St ($St < 0.2$), a drag producing wake is generated. For values approximately between $0.2 < St < 0.25$ a neutral wake is encountered and for values higher than $St = 0.3$, we are in the presence of a thrust producing wake. In this figure, it is also observed that for Strouhal numbers $St > 0.5$, the wake start to become deflected, becoming asymmetric and in some cases aperiodic, as described later. It is important to note that these classifications are based purely on the observed vortex positions. Quantitative measurements, as we will be presenting later, suggest that these classifications are fairly conservative, with thrust generation occurring at Strouhal numbers as low as $St = 0.2$.

The deflected wake topology (see figure 7.10), apparently was first observed experimentally by Bratt [23], but he did not comment on these deflected wakes. In fact, it seems that they were never again reported until 1998, when Jones *et al.* [94] studied them in greater detail, both experimentally and computationally. Numerically, the deflection angle of the wake is determined by the starting direction of the heaving motion, *i.e.*, if the heaving motion starts from the bottommost position, the wake is deflected upwards and if the heaving motion starts from the topmost position, the wake is deflected downwards, as shown in figure 7.10.

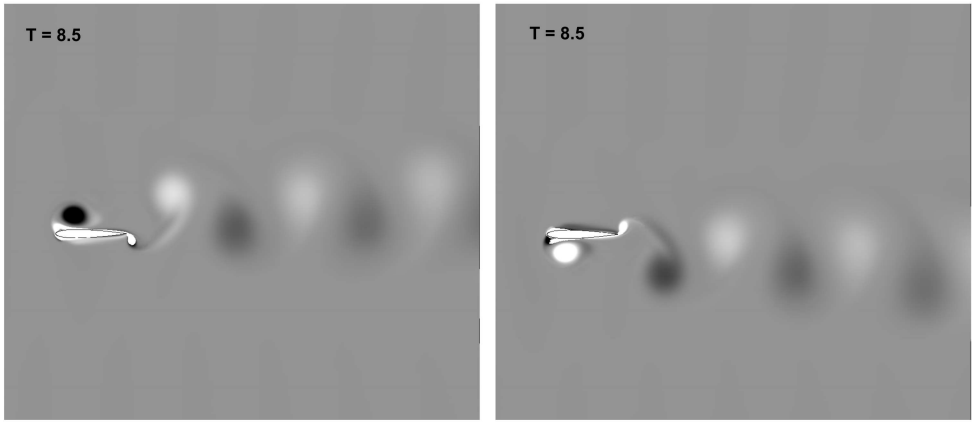

Figure 7.10: *Deflected wake (vorticity contours). In the left figure the wake is deflected upwards (the motion was started from the bottommost position), while in the right figure the wake is deflected downwards (the motion was started from the topmost position). Flapping parameters for both cases:* $Re = 1100$, $St = 0.5$, $h_a = 0.3$.

In a numerical study performed by Emblemsvag *et al.* [49], it was reported that as the Strouhal number increases, the vortices tend to shed in pairs (vortex dipoles) and form a deflected wake. This same observation was also confirmed in the present study. In figure 7.11, we plot the horizontal velocity profile as the Strouhal number increases (which reflects the wake deflection). The time average velocity profiles were measured at a distance equals to 6 times the airfoil chord away from the trailing edge.

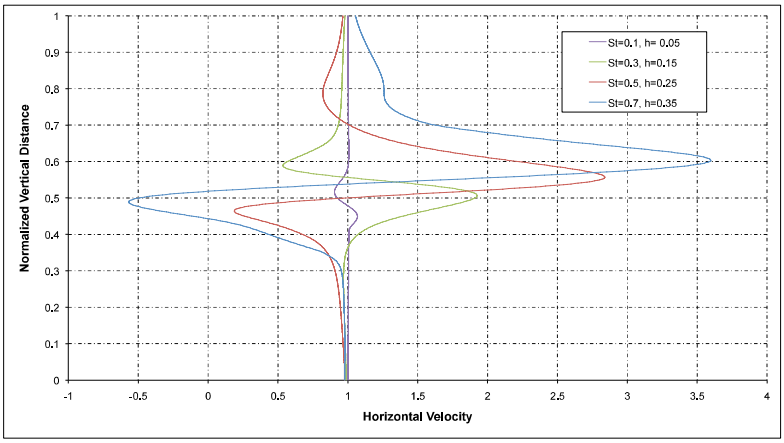

Figure 7.11: *Horizontal velocity profile evolution as function of the Strouhal number.*

Besides the obvious wake deflection, there are several other interesting features of this solution. At this high Strouhal numbers a substantial thrust coefficient is produced, with fairly low propul-

sive efficiency. What is interesting is that an average lift is also produced due to an induced angle of attack created by the presence of the deflected wake (see figure 7.12). In general, the deflected wake topologies were found to be highly reproducible. The simulations were run for a long time and it was observed that for Strouhal number values between $0.5 < St < 0.7$, they do appear to be converging toward a periodic asymptote.

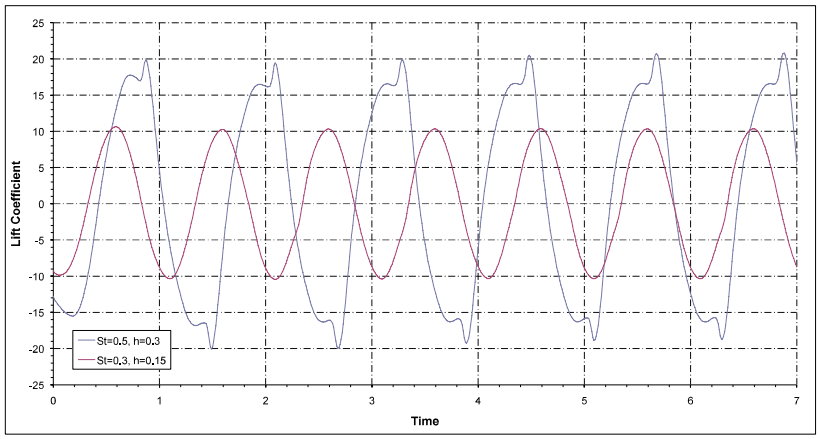

Figure 7.12: *Time dependent lift coefficient for two different heaving cases. Notice that for the case* $St = 0.5\,(h = 0.3)$*, the lift coefficient evolution is not symmetric about the horizontal mean line, this is due to the angle of attack induced by the deflected wake, the bumps on the lift curve are due to the dynamic stall* ($\overline{c_l} = 0.10923$)*. For the case* $St = 0.3\,(h = 0.15)$ *the lift evolution is symmetrical about the horizontal mean line* ($\overline{c_l} = 0.00242$)*.*

An interesting phenomenon related to the deflected wake is the aperiodic jet-switching phenomenon, where the direction in which the wake is deflected is observed to switch from upward to downward deflection (or downward to upward, depending on the starting direction of the heaving motion). This switching was reported by Jones *et al.* [94], for high-frequency heaving in water tunnel experiments, but they were not able to reproduce it using their inviscid unsteady panel code. Lewin and Haj-Hariri [108], were apparently the firsts to numerically simulate the jet-switching phenomenon. In the present study, we were able to simulate the jet-switching phenomenon but for values different from those used by Lewin and Haj-Hariri; the fact that we were not able to reproduce the same results of Lewin and Haj-Hariri is probably due to the differences with the grid and the numerical method. It is worth to mention that from our simulations we were not able to determine if the switching is random or periodic, basically due to the fact that the simulations have to be run for long times due to the aperiodic nature of the phenomenon, as noted by Heathcote and Gursul [69]. In their work, they presented experimental evidence that in fact, the jet-switching phenomenon is quasiperiodic. They found the period of switching to be two orders of magnitude greater than the heaving period. These large periods are clearly challenging for numerical simulations, and may be the reason for the lack of numerical simulations displaying the phenomenon. At the high Strouhal number values where the deflected wake is encountered, the vortices shed from the trailing edge (TEV) come very close to one another and start to interact with each other forming a vortex pair, which apparently seems to be the reason for the phenomenon. The leading edge vortex (LEV) has also an influence on the occurrence of this phenomenon, but in general the TEV seems to be the dominating factor.

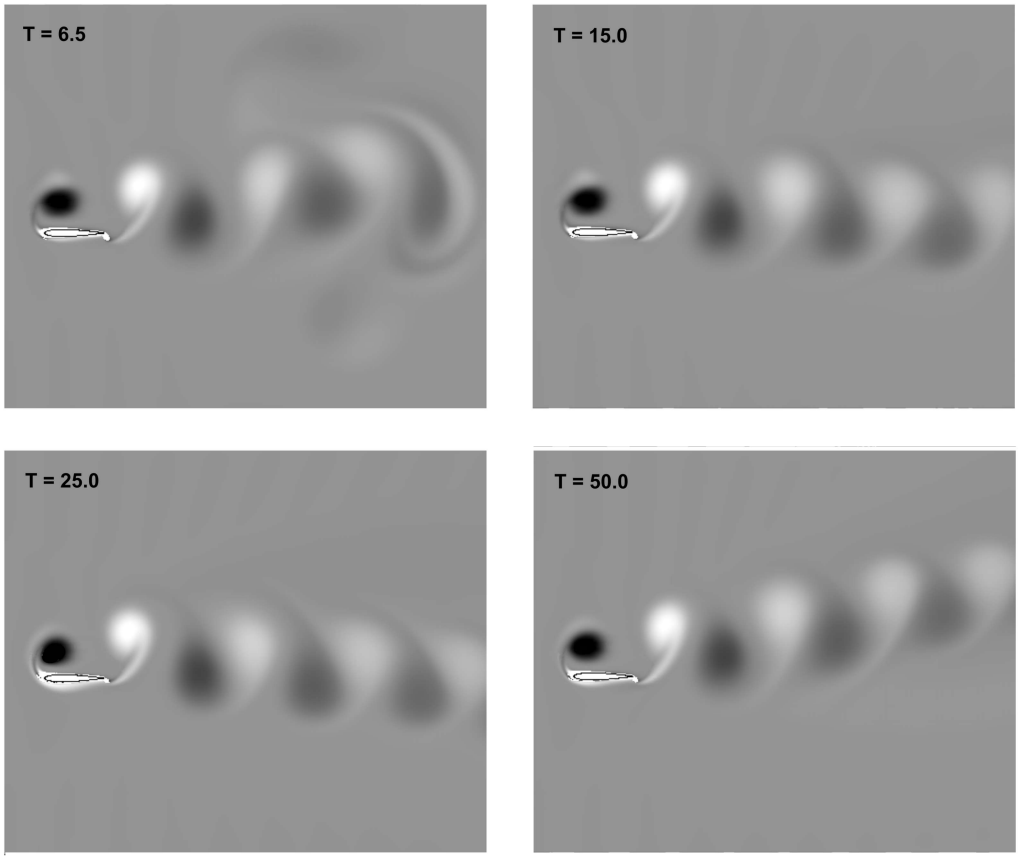

Figure 7.13: *Jet-switching phenomenon (vorticity contours). Notice how the wake first goes to the upward position, then goes to the downward position and then returns to the upward position. Also notice that the wake deflection angles are different for the upward and downward deflection. Flapping parameters:* $Re = 1100$, $St = 0.9$, $h_a = 0.45$.

In order to fully study our parameter space (f_h, h_a) and to isolate the optimal aerodynamic performance, we construct a contour map of propulsive efficiency against Strouhal number and heaving amplitude (nearly 100 simulations), as shown in figure 7.15. In this figure, we can clearly identify two regions of maximum efficiency, one corresponding to $0.25 < St < 0.3$ and a second one corresponding to $0.35 < St < 0.4$. Cross-referencing this figure with its corresponding contour map of thrust coefficient (figure 7.16), we observe that these two regions correspond to a *"low thrust"* and a *"high thrust"* areas, respectively. Usually, the first one is not significant for practical applications because the thrust coefficient is often very small, whereas the second peak is associated with higher thrust coefficient (in our case the coefficient value of the *"high thrust"* area is approximately twice the value of the *"low thrust"* area). In figure 7.17, we present the contour map of input power coefficient; in this figure we can observe that both the *"low thrust"* and *"high thrust"* areas are in the range of low input power coefficient. Thrust coefficients values higher that the values corresponding to the highest efficiencies are in fact obtained, but at the cost of very high input power coefficient (as seen in figure 7.17) and hence the propulsive efficiency is very low (figure 7.15), making this range of high thrust production unattractive for practical

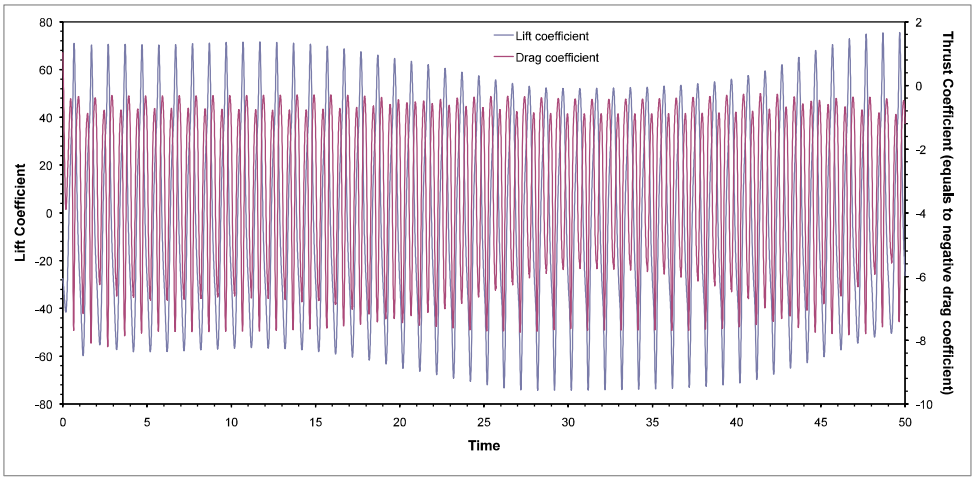

Figure 7.14: *Lift coefficient and drag coefficient time histories for the jet-switching wake. Flapping parameters:* $Re = 1100$, $St = 0.9$, $h_a = 0.45$. *Negative values of drag coefficient indicate thrust production.*

application.

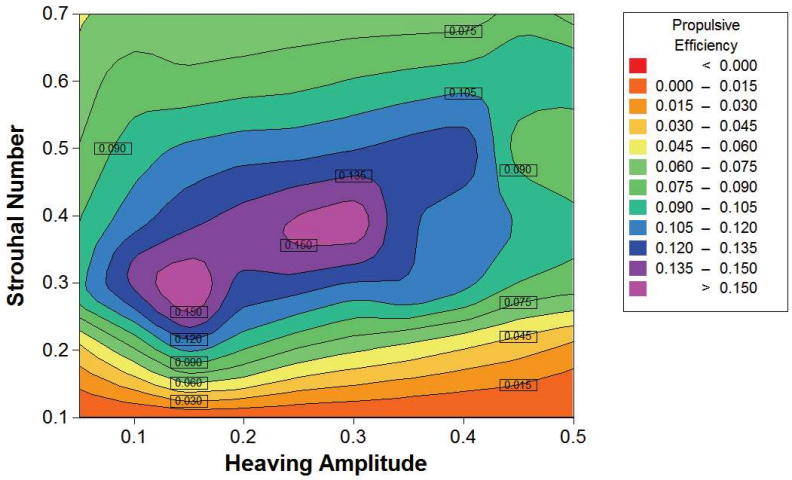

Figure 7.15: *Contour map of propulsive efficiency vs. Strouhal number and heaving amplitude.*

All these qualitative and quantitative results agree with the hypothesis that : *"flying and swimming animals cruise at a Strouhal number tuned for high power efficiency"* [182]. The enhanced efficiency range was found to be between Strouhal number values corresponding to $0.2 < St < 0.4$, which agrees with the observations of Nudds *et al.* [136], Rohr and Fish [155], Taylor *et al.* [182] and Triantafyllou *et al.* [193]. From this extensive numerical experiment, we can also confirm that the Strouhal number (based on the total trailing edge excursion or heaving amplitude) is enough for wake topology characterization, but cannot be used as a single parameter to describe

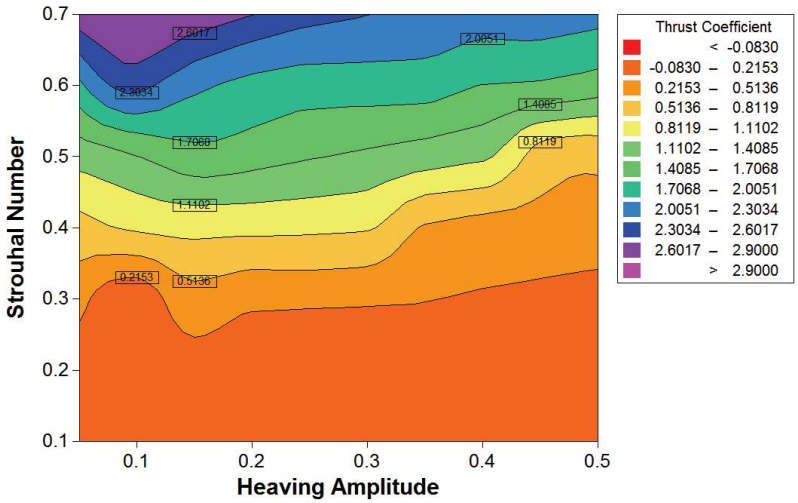

Figure 7.16: *Contour map of thrust coefficient vs. Strouhal number and heaving amplitude.*

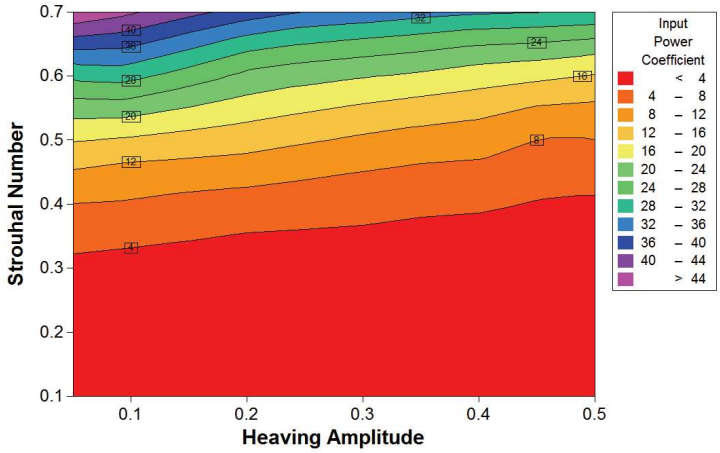

Figure 7.17: *Contour map of input power coefficient vs. Strouhal number and heaving amplitude.*

the flow in terms of maximum efficiency. The reduced frequency k is also necessary to have a complete description of the aerodynamic performance.

7.3 Leading Edge Vortex Shedding and Frequency Dependence

From figure 7.15, it can be observed that very different behaviors on the aerodynamic performance can be obtained between high heaving frequencies (low heaving amplitudes) and low heaving frequencies (high heaving amplitudes). The explanation for this frequency dependence will be studied hereafter.

7.3. LEADING EDGE VORTEX SHEDDING AND FREQUENCY DEPENDENCE

Let us proceed to compute the instantaneous distribution of lift coefficient $c_l\,(x/c)$ and thrust coefficient $c_t\,(x/c)$ on the airfoil surface due solely to the pressure. These quantities are computed as follows

$$\begin{aligned} c_l\,(x/c) &= -c_p cos\,(\theta_s) \\ c_t\,(x/c) &= -c_p sin\,(\theta_s) \end{aligned} \tag{7.1}$$

where c_p is the local pressure coefficient on the airfoil surface, and θ_s is the local angle of the airfoil surface with respect to the horizontal axis. The instantaneous distribution of moment coefficient $c_m\,(x/c)$ and input power coefficient $c_P\,(x/c)$ on the airfoil surface are computed as follows

$$\begin{aligned} c_m\,(x/c) &= -c_l\,(x/c)\left(\frac{x-x_p}{c}\right) - c_t\,(x/c)\left(\frac{y-y_p}{c}\right) \\ c_P\,(x/c) &= -c_l\,(x/c)\left(\frac{\dot{y}(t)}{U_\infty c}\right) - c_m\,(x/c)\left(\frac{\dot{\alpha}(t)}{U_\infty}\right) \end{aligned} \tag{7.2}$$

Note that for pure heaving motion the pitch rate is $\dot{\alpha}(t) = 0$, so that the input power coefficient distribution is dependent only on the lift coefficient distribution and the vertical motion of the airfoil.

In figure 7.18, we show the pressure field around a heaving airfoil for eight different instants in time during period of the signal (which corresponds to the upstroke phase). As it can be seen in this figure, there is a vortex that separates from the leading edge and is convected downstream over the airfoil surface; obviously, the low pressure in the vortex core have an effect on the aerodynamic performance that will be studied hereafter. Halfway through the period a vortex is formed at the leading edge and proceeds along the lower side of the airfoil, eventually detaching at the trailing edge.

By using equations 7.1 and 7.2, we proceed to compute the instantaneous lift coefficient, thrust coefficient, moment coefficient and input power coefficient. In figures 7.19 and 7.20 we show the pressure coefficient distribution on the airfoil surface and the regions on the airfoil surface responsible for the greatest development of thrust at four different instants during the upstroke. The flapping parameters for this case are $Re = 1100$, $St = 0.35$, $h_a = 0.40$ and $f = 0.4375$ ($k = 1.3744325$).

In figure 7.18, the flow separates at the leading edge and forms a leading edge vortex (LEV), which is convected downwards; this LEV is a spike of locally low pressure. The vortex is convected downstream over the airfoil and diffuses as it moves towards the trailing edge. As long as the vortex remains upstream of the point of maximum thickness of the airfoil, it contributes towards thrust, however as it travels aft of this point its contribution changes sharply and drag is produced.

In figures 7.21, 7.22 and 7.23, similar results to those of the previous case are illustrated. In this case the flapping parameters are $Re = 1100$, $St = 0.35$, $h_a = 0.15$, $f = 1.166667$ ($k = 3.665166$). In figure 7.21, the pressure field for eight different instants during the upstroke are shown; also in this case a LEV forms and separates, but this time it is not convected all the way downstream. In this case, the vortex remains more time in the nose region of the airfoil and its contribution to the thrust is higher.

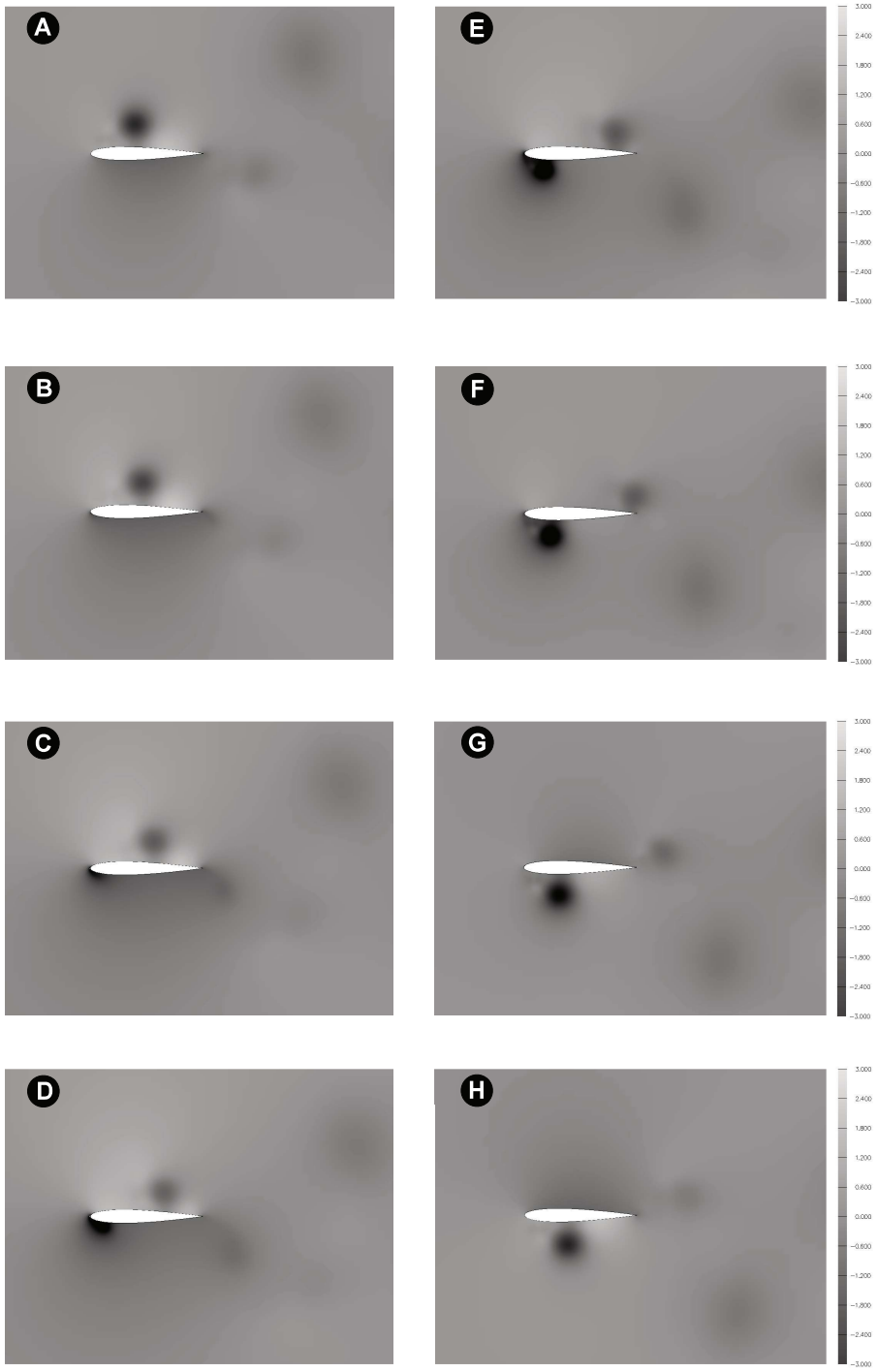

Figure 7.18: *Pressure field during upstroke. Flapping parameters:* $Re = 1100$, $St = 0.35$, $h_a = 0.40$, $f = 0.4375$ ($k = 1.3744325$). *The sequence is from A (bottommost position) to H (topmost position), where: A)* $t = 13.725$, *B)* $t = 13.860$, *C) 14.0, D) 14.168, E) 14.345, F) 14.476, G) 14.652, H) 14.828.*

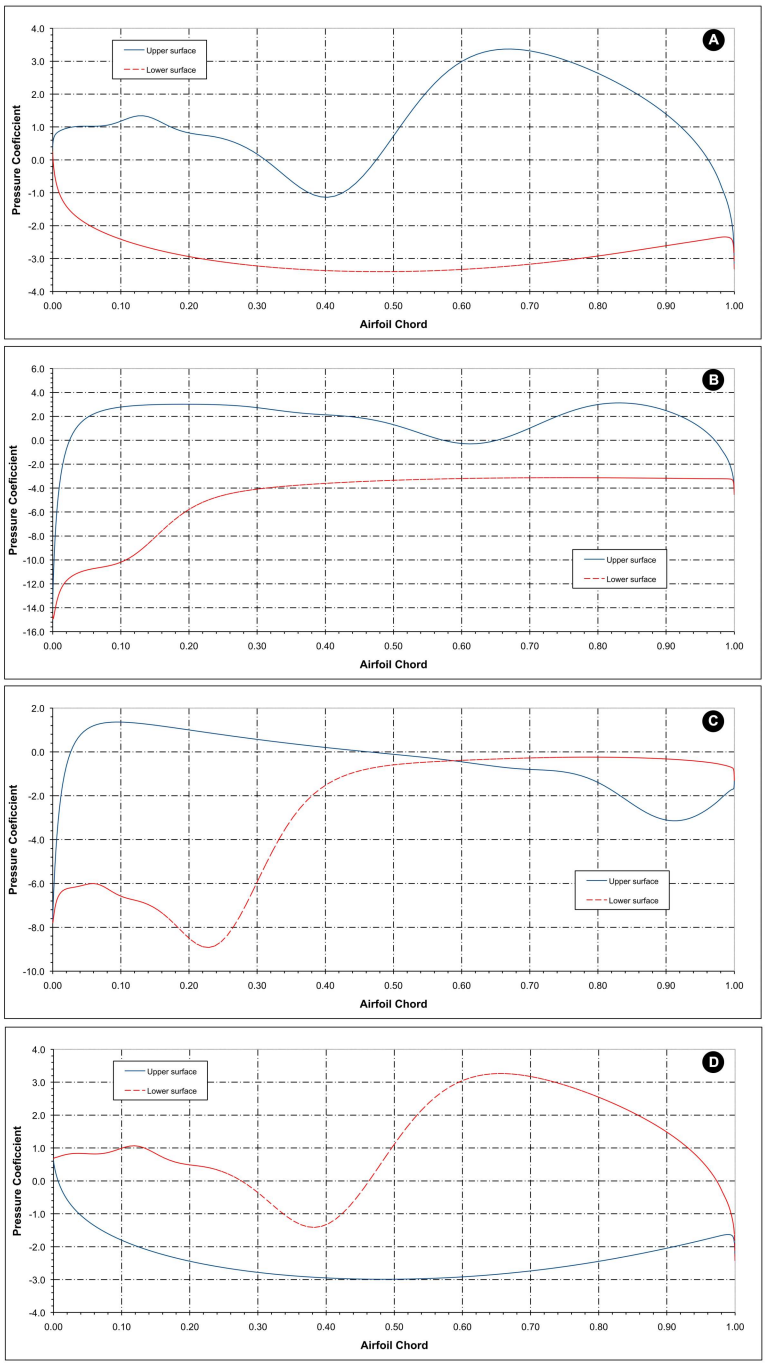

Figure 7.19: *Pressure coefficient distribution on the airfoil surface. Flapping parameters:* $Re = 1100$, $St = 0.35$, $h_a = 0.40$, $f = 0.4375$ ($k = 1.3744325$). *The sequence is from A (bottommost position) to D (topmost position). The pressure coefficient* c_p *was measured at the following instants: A)* $t = 13.728$, *B)* $t = 14.124$, *C) 14.476, D) 14.828.*

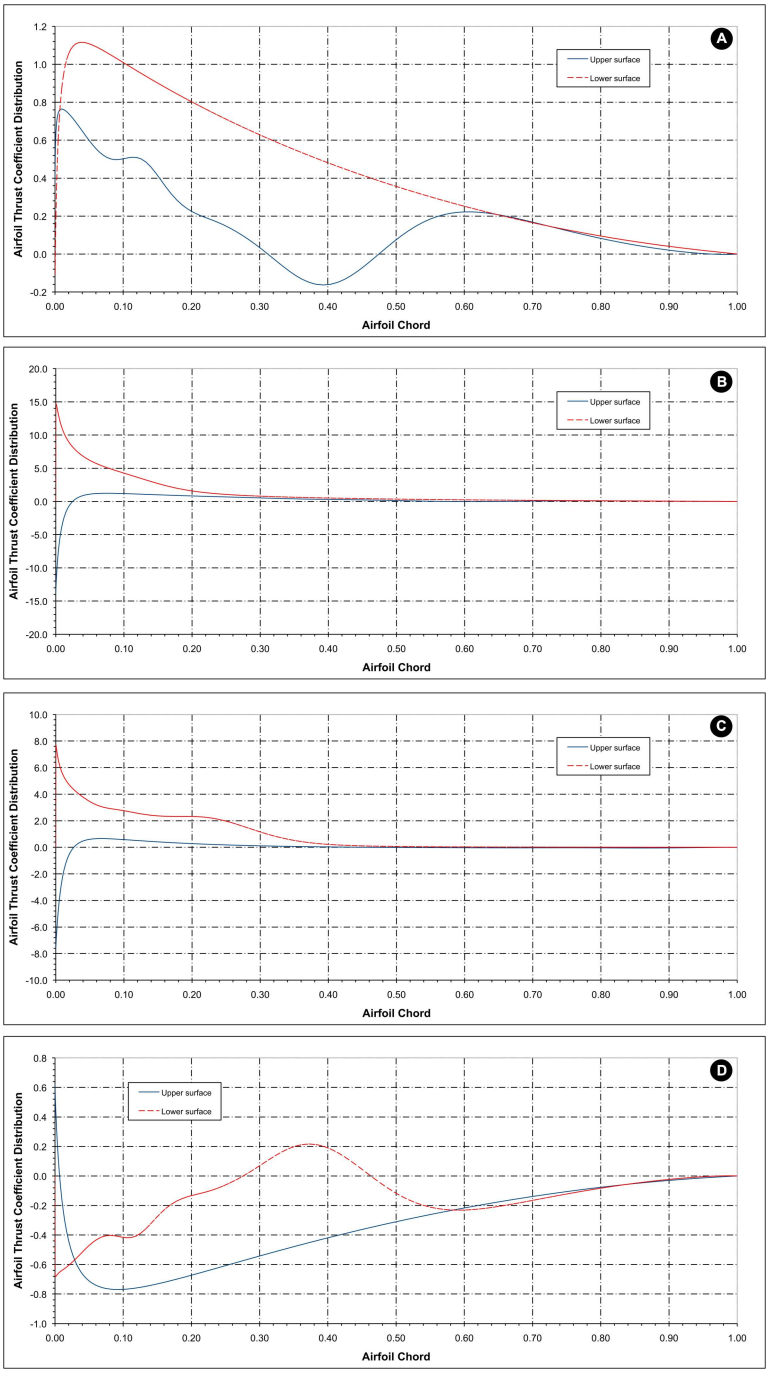

Figure 7.20: *Thrust coefficient distribution on the airfoil surface. Flapping parameters:* $Re = 1100$, $St = 0.35$, $h_a = 0.40$, $f = 0.4375$ ($k = 1.3744325$). *The sequence is from A (bottommost position) to D (topmost position). The thrust coefficient distribution* $c_t(x/c)$ *was measured at the following instants: A)* $t = 13.728$, *B)* $t = 14.124$, *C) 14.476, D) 14.828.*

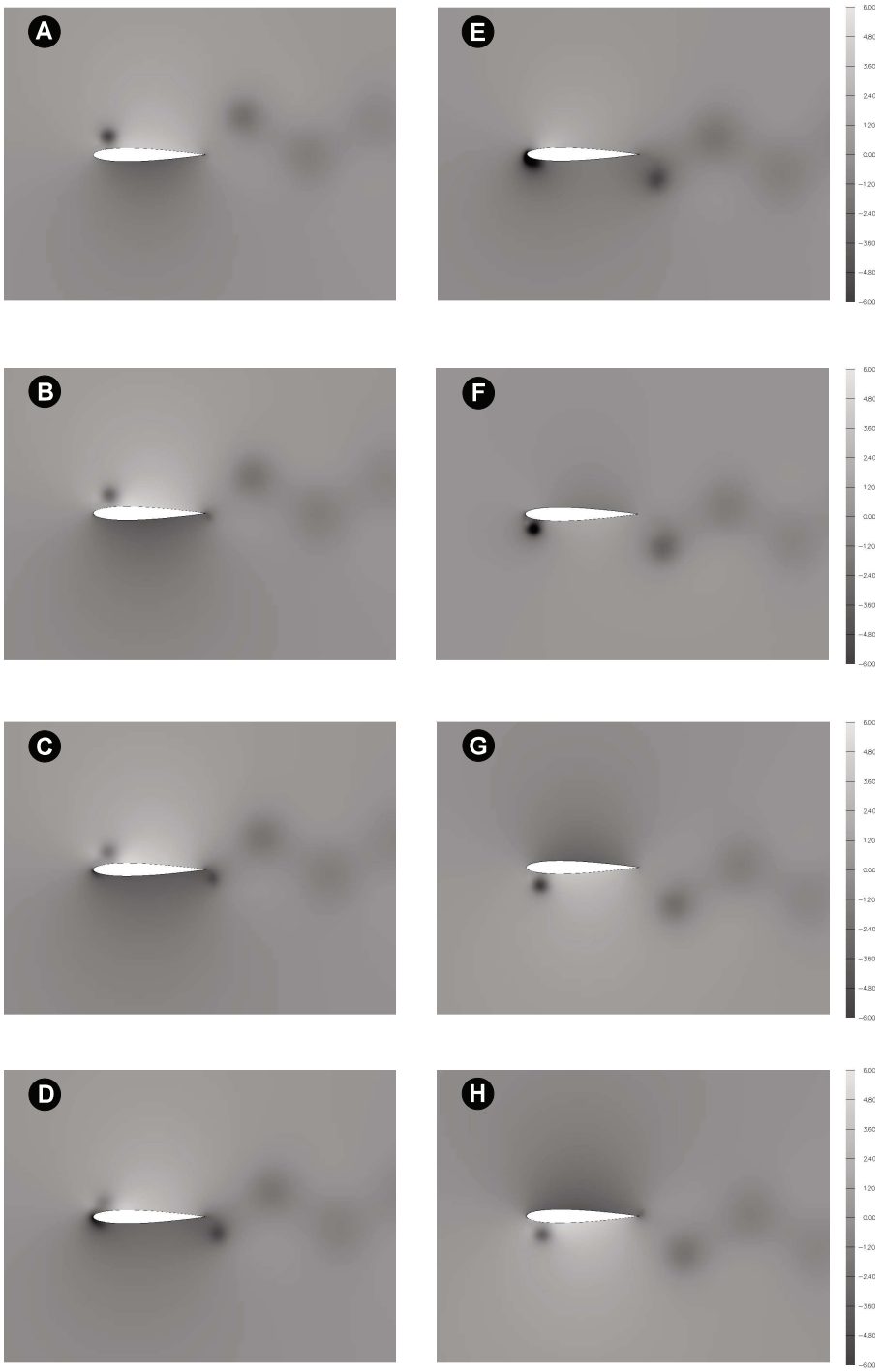

Figure 7.21: *Pressure field during upstroke. Flapping parameters:* $Re = 1100$, $St = 0.35$, $h_a = 0.15$, $f = 1.166667$ ($k = 3.665166$). *The sequence is from A (bottommost position) to H (topmost position), where: A)* $t = 5.120$, *B)* $t = 5.184$, *C) 5.248, D) 5.317, E) 5.376, F) 5.456, G) 5.536, H) 5.6.*

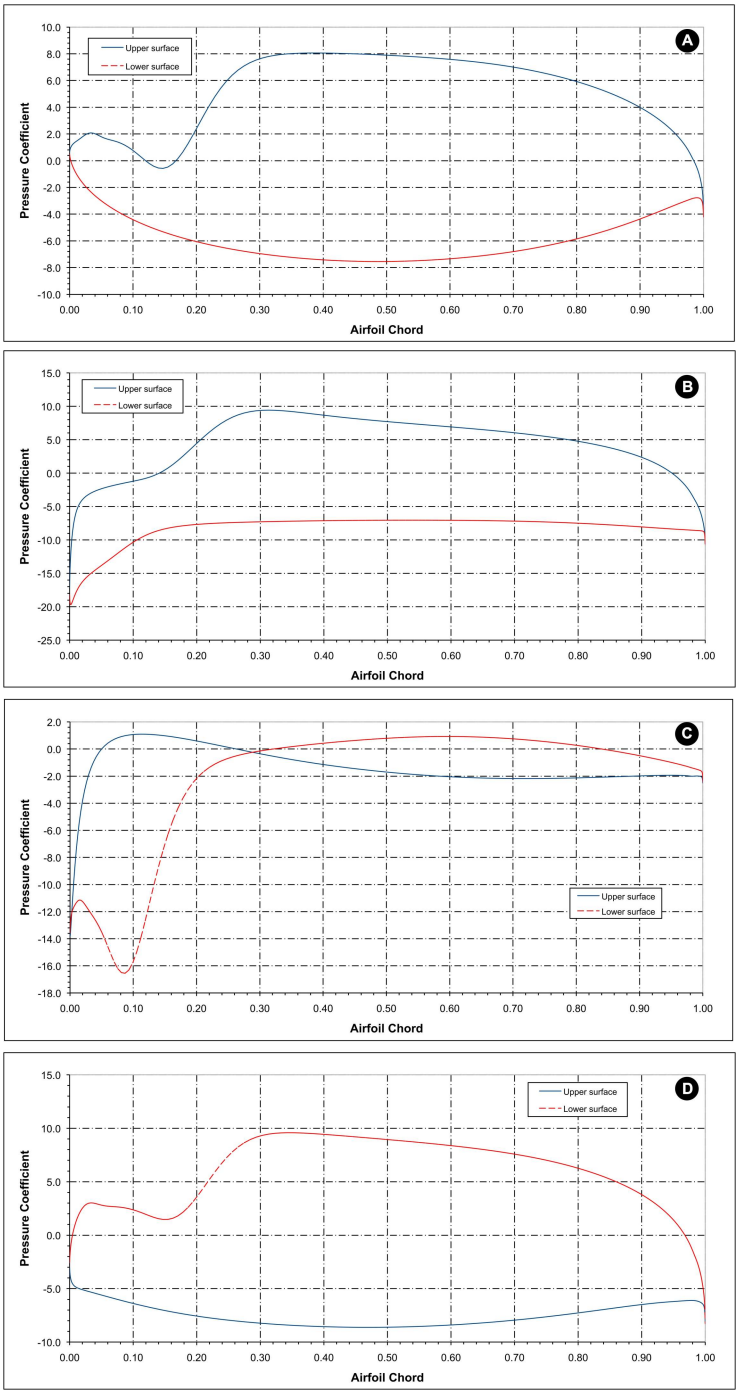

Figure 7.22: *Pressure coefficient distribution on airfoil surface. Flapping parameters:* $Re = 1100$, $St = 0.35$, $h_a = 0.15$, $f = 1.166667$ ($k = 3.665166$). *The sequence is from A (bottommost position) to D (topmost position). The pressure coefficient* c_p *was measured at the following instants: A)* $t = 5.120$, *B)* $t = 5.280$, *C) 5.456, D) 5.6.*

By comparing figures 7.18 and 7.21, it is evident that the effect of the LEV separation becomes

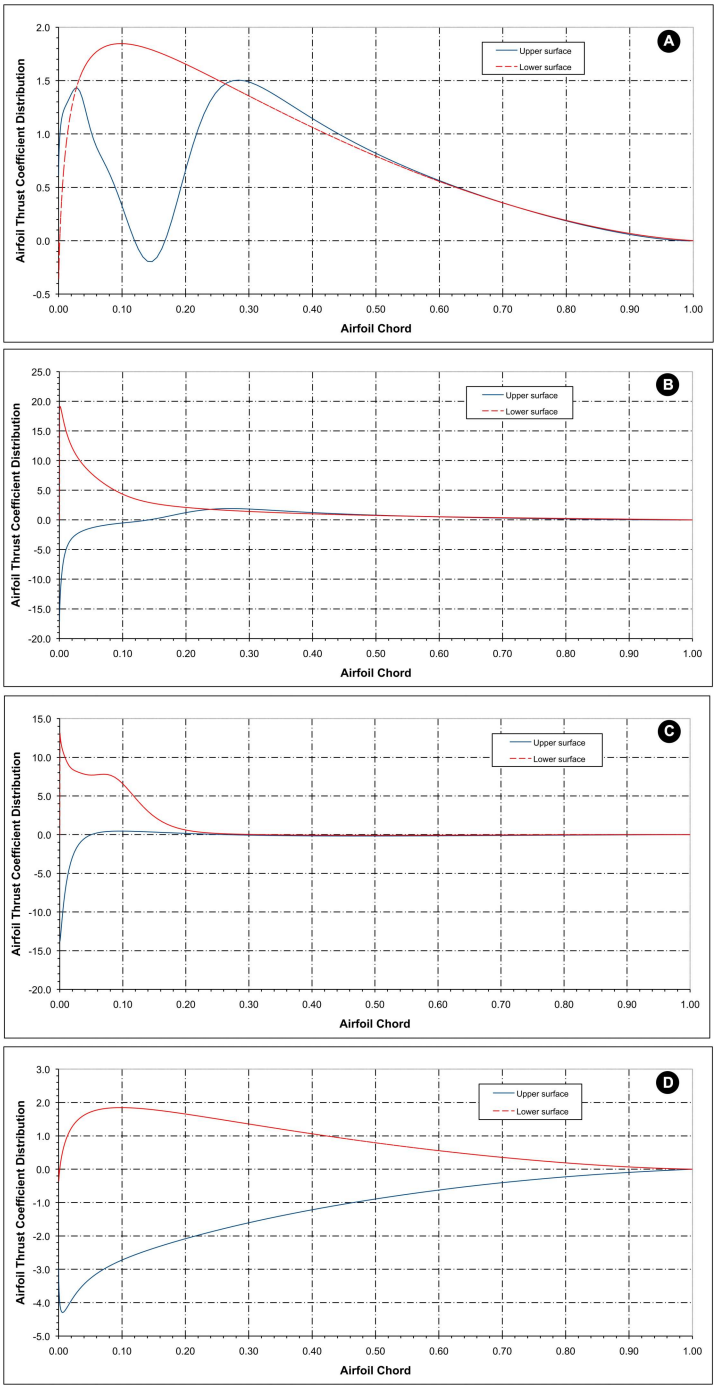

Figure 7.23: *Thrust coefficient distribution on airfoil surface. Flapping parameters:* $Re = 1100$, $St = 0.35$, $h_a = 0.15$, $f = 1.166667$ ($k = 3.665166$). *The sequence is from A (bottommost position) to D (topmost position). The thrust coefficient distribution* $c_t(x/c)$ *was measured at the following instants: A)* $t = 5.120$, *B)* $t = 5.280$, *C) 5.456, D) 5.6.*

much less pronounced as the flapping frequency f (and hence the reduced frequency k) is increased. Both the size of the vortex and its effect on the airfoil surface pressure distribution are reduced as the frequency k is increased (while holding St constant). Thus leading edge separation introduces a frequency dependence into the results. This provides a mechanism of optimal selection of heaving frequency (in the sense of maximum propulsive efficiency), as discussed by Wang [207].

As the reduced frequency k increases, there is less time for the vortex to form and to travel downstream along the airfoil past the point of maximum thickness, where it contributes to drag rather than to thrust generation, hence lowering the propulsive efficiency. The LEV also has a smaller relative effect on the airfoil surface pressure distribution at higher k, because the pressure extremes developed around the airfoil during the motion cycle are greater with increasing k (note the increased pressure coefficient by comparing figures 7.22 and 7.19). This is consistent with the peak lift coefficient increasing roughly linearly with k, as shown in figure 7.24.

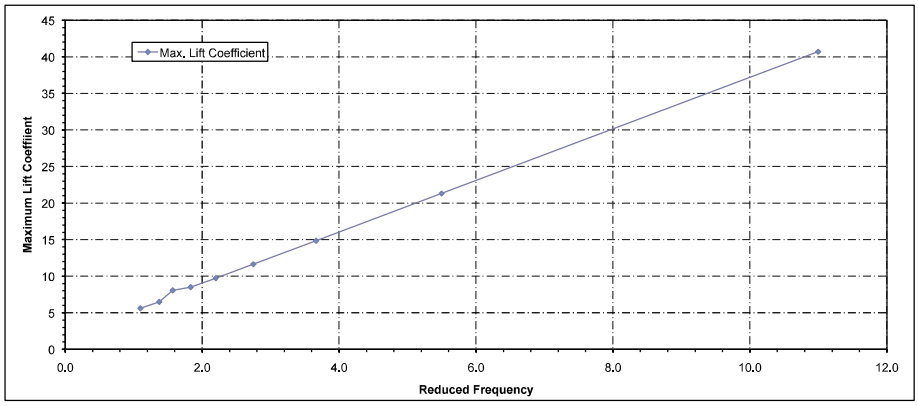

Figure 7.24: *Peak lift coefficient versus reduced frequency k. Flapping parameters:* $Re = 1100$, $St = 0.35$.

It is worth noting that a large majority of the thrust is generated at the nose of the airfoil, particularly at low k, consistent with the observations of Tuck [195] and Lee *et al.* [106]. From these results, it is also evident that the wake roll-up has only a secondary effect on the thrust generated and this is in agreement with the findings of Hall and Hall [64], where the effect of wake roll-up on the forces generated by a heaving flat plate was studied. They showed in [64] that the time histories of the lift coefficient for the prescribed-wake and free-wake models were virtually identical, with only minor differences in peak values. At the frequency tested, the non-linear roll-up of the wake has only a minor effect on the forces felt on the airfoil surface.

Clearly, the separation and convection of the LEV is crucial in determining the aerodynamic behavior of the airfoil. The effect of the LEV on the aerodynamic performance is particularly pronounced for pure heaving airfoils. For coupled heaving-and-pitching motions, where the orientation of the airfoil surface is controlled by the relative amplitudes and phases of the motion, the LEV may create positive thrust for much longer portions of the flapping cycle, thus contributing towards the propulsive efficiency. Coupled heaving-and-pitching motion is explored in the next section.

7.4 Flapping airfoils (Coupled Heaving-and-Pitching Motion)

This section is devoted to the study of airfoils undergoing flapping motion (coupled heaving-and-pitching motion). The main goal is to study the effect of the flapping variables (heaving amplitude h_a, pitching amplitude α_a, heaving frequency f_h, pitching frequency f_α and phase angle φ) on the aerodynamic behavior.

As in the pure heaving case, let us first take a look at the flapping motion (eq. 2.21 and eq. 2.22) and at the evolution of lift and thrust coefficients with time for a single flapping case. In figure 7.25 the heaving-and-pitching kinematics is plotted, in this figure one period consists of an up and down stroke. As in the heaving case, since the airfoil is symmetric and is oscillating symmetrically about the mean horizontal line, we expect a symmetrical lift evolution. The frequency of the thrust coefficient is twice that of the lift coefficient because thrust is generated in both the up and down strokes.

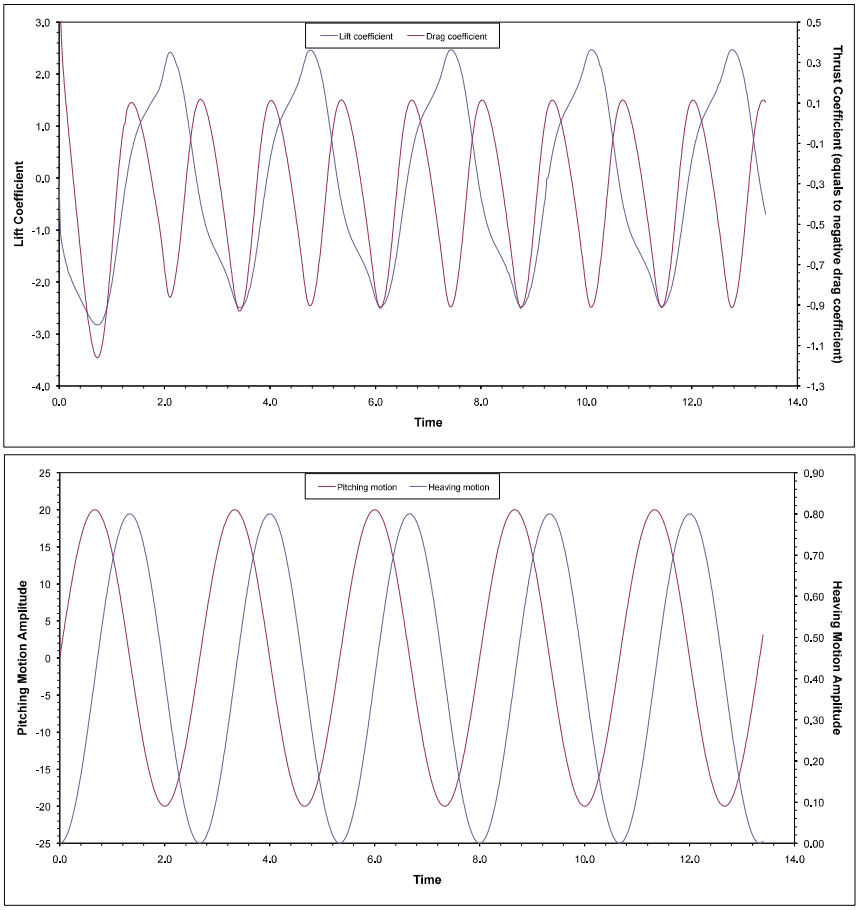

Figure 7.25: *Top figure: time dependent thrust and lift coefficients (where negative values of drag coefficient indicate thrust production). Bottom figure: Heaving and pitching kinematics. Flapping parameters:* $Re = 1100, St = 0.3, h_a = 0.4$, $\alpha_a = 20°$, $\varphi = 90°$ ($\overline{c_t} = 0.354186$, $\overline{c_l} = -0.001725$).

7.4.1 Effect of Maximum Pitching Angle

Hereafter, we conduct a parametric study to determine the best maximum pitching angle α_a for operating with the highest efficiency. In this section, we vary the maximum pitching angle α_a from 5 to 40 degrees, and we fix the pitching and heaving frequency $f_h = f_\alpha = f$, heaving amplitude h_a and phase angle φ. The Strouhal number was set to $St = 0.3$, which corresponds to a maximum efficiency peak in figure 7.15.

Case number	f(Hz)	h_a	$\alpha_a(^\circ)$	$\varphi(^\circ)$	k	St
2DF1-1	0.15	1.0	5.0	90.0	0.7096	0.3
2DF1-2	0.15	1.0	10.0	90.0	0.7096	0.3
2DF1-3	0.15	1.0	15.0	90.0	0.7096	0.3
2DF1-4	0.15	1.0	20.0	90.0	0.7096	0.3
2DF1-5	0.15	1.0	25.0	90.0	0.7096	0.3
2DF1-6	0.15	1.0	30.0	90.0	0.7096	0.3
2DF1-7	0.15	1.0	35.0	90.0	0.7096	0.3
2DF1-8	0.15	1.0	40.0	90.0	0.7096	0.3

Table 7.2: *Kinematics parameters for the study of the effect of maximum pitching angle on flapping airfoils aerodynamic performance. Flapping parameters:* $Re = 1100$, $St = 0.3$, $h_a = 1.0$.

Figure 7.26 shows the average thrust coefficient and propulsive efficiency as function of the maximum pitching angle α_a. In this figure, a maximum in the average thrust coefficient can be identified between $15 < \alpha_a < 25$ degrees, whereas a maximum in the propulsive efficiency can be identified around $\alpha_a = 30$ degrees.

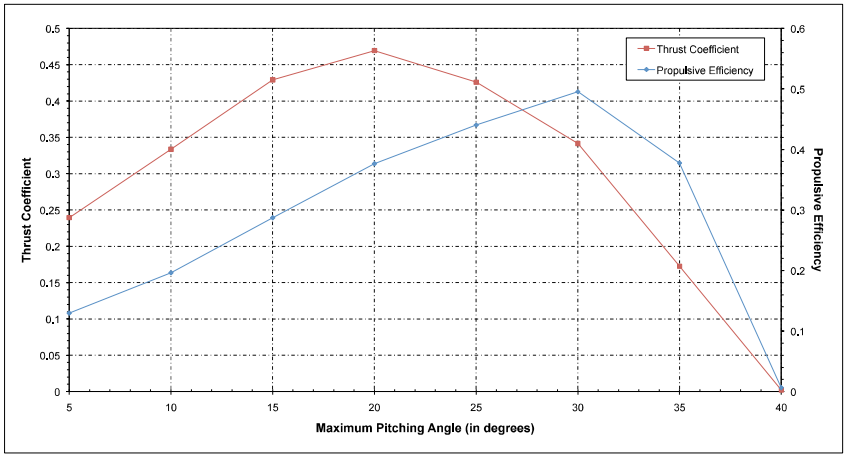

Figure 7.26: *Average thrust coefficient and propulsive efficiency versus maximum pitching angle. Flapping parameters:* $Re = 1100$, $St = 0.3$, $h_a = 1.0$.

To choose a point of operation, one has to balance the need of high thrust without sacrificing propulsive efficiency. Maximum efficiency is obtained at a maximum pitching angle $\alpha_a = 30$ degrees, while maximum thrust is obtained at a maximum pitching angle $\alpha_a = 20$ degrees. There-

fore, a maximum pitching angle value between $20 < \alpha_a < 30$ degrees seems to be a reasonably good choice for operating at high thrust coefficient and propulsive efficiency values.

7.4.2 Effect of Heaving Amplitude

Let us now study the effect of heaving amplitude on the aerodynamic performance. The parameters used for this study are shown in table 7.3, where we fix the Strouhal number value to $St = 0.3$ and we vary the heaving amplitude h_a and the flapping frequency $f_h = f_\alpha = f$, the results are shown for five different values of maximum pitching amplitude (15, 20, 25, 30 and 35 degrees).

Case number	$\alpha_a(^\circ)$	$\varphi(^\circ)$	h_a	f (Hz)	St
2DF2-1	15.0	90.0	$0.1 < h_a < 1.4$	$0.107143 < f < 1.50$	0.3
2DF2-2	20.0	90.0	$0.2 < h_a < 1.4$	$0.107143 < f < 0.75$	0.3
2DF2-3	25.0	90.0	$0.2 < h_a < 1.4$	$0.107143 < f < 0.75$	0.3
2DF2-4	30.0	90.0	$0.2 < h_a < 1.6$	$0.093750 < f < 0.75$	0.3
2DF2-5	35.0	90.0	$0.2 < h_a < 1.6$	$0.093750 < f < 0.75$	0.3

Table 7.3: *Flapping parameters for the study of the effect of heaving amplitude h_a on the aerodynamic performance.*

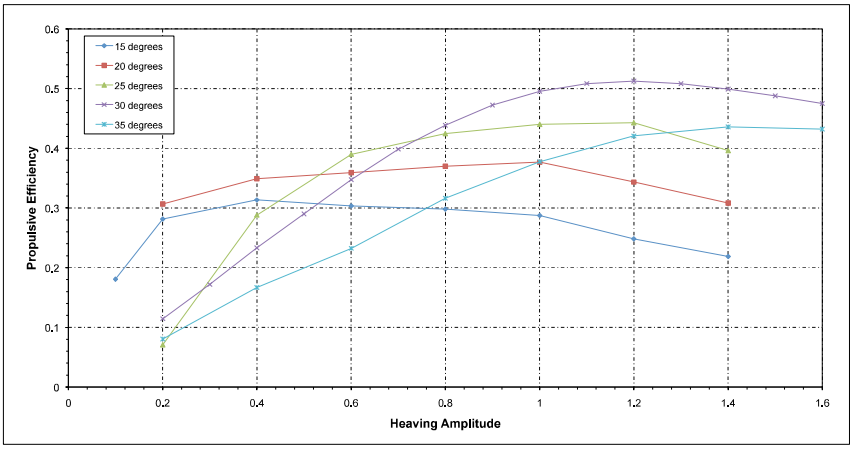

Figure 7.27: *Propulsive efficiency versus heaving amplitude. Flapping parameters: $Re = 1100$, $St = 0.3$.*

As observed in figure 7.27, the propulsive efficiency increases with the heaving amplitude, until it reaches a maximum value where from which point on it start to decrease. For the cases shown in figure 7.27, the maximum propulsive efficiency is obtained around $\alpha_a = 30$ degrees and $h_a = 1.2$. Figures 7.28 and 7.29 show the corresponding thrust coefficient and input power coefficient variations with the heaving amplitude. In figures 7.28 we can observe that at low heaving amplitude values we obtain high thrust coefficients, but at the cost of very high input power coefficient values, making this range of amplitudes unattractive for practical applications. For this case, the best operating point (in terms of propulsive efficiency) is found for heaving amplitude values between $0.8 < h_a < 1.2$.

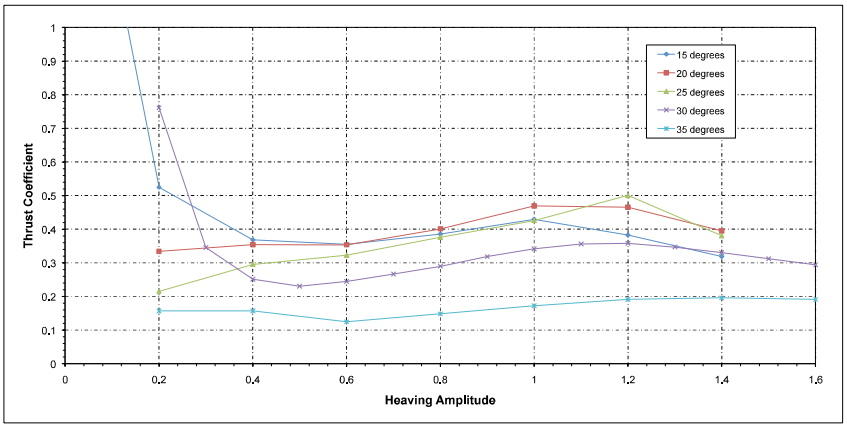

Figure 7.28: *Average thrust coefficient versus heaving amplitude. Flapping parameters:* $Re = 1100$, $St = 0.3$.

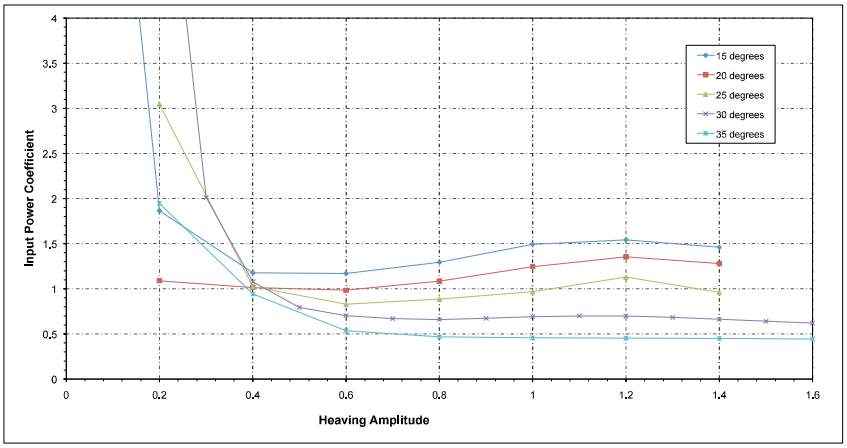

Figure 7.29: *Average input power coefficient versus heaving amplitude. Flapping parameters:* $Re = 1100$, $St = 0.3$.

7.4.3 Effect of Strouhal Number

As observed in the study of pure heaving motion, the Strouhal number is a crucial parameter in the thrust generation mechanism, and even the slightest change in the amplitude or frequency can alter quite significantly thrust and efficiency. In this case, we fix the maximum pitching angle to $\alpha_a = 20$ degrees and we vary the heaving amplitude h_a and the flapping frequency $f_h = f_\alpha = f$, the results are shown for Strouhal number values equal to 0.2, 0.3 and 0.4.

In figure 7.30 the results for the propulsive efficiency are plotted for three values of Strouhal number. In this figure, the value of Strouhal number $St = 0.2$, corresponds to low values of thrust coefficient (almost in the neutral regime), while the other two values correspond to high thrust coefficient values (see figure 7.31). As the Strouhal number rises above $St = 0.2$, the maximum propulsive efficiency values are reached very fast with the increase of the heaving amplitude, until reaching a maximum value where they begin to decrease. The increase in the average thrust

Case number	$\alpha_a(^\circ)$	$\varphi(^\circ)$	h_a	f (Hz)	St
2DF3-1	20.0	90.0	$0.2 < h_a < 1.4$	$0.071428 < f < 0.50$	0.2
2DF3-2	20.0	90.0	$0.2 < h_a < 1.4$	$0.107143 < f < 0.75$	0.3
2DF3-3	20.0	90.0	$0.2 < h_a < 1.4$	$0.142857 < f < 1.00$	0.4

Table 7.4: *Flapping parameters for the study of the effect of Strouhal number St on the aerodynamic performance.*

coefficient and input power coefficient with the Strouhal number (see figures 7.31 and 7.32) can be attributed to the increased pressure differences due to the higher heaving velocity of the airfoil as St increases, thereby resulting in higher lift and thrust coefficients. In this case, the best operating point (in terms of propulsive efficiency) corresponds to a Strouhal number value equal to $St = 0.3$, with a corresponding heaving amplitude value between $0.8 < h_a < 1.2$.

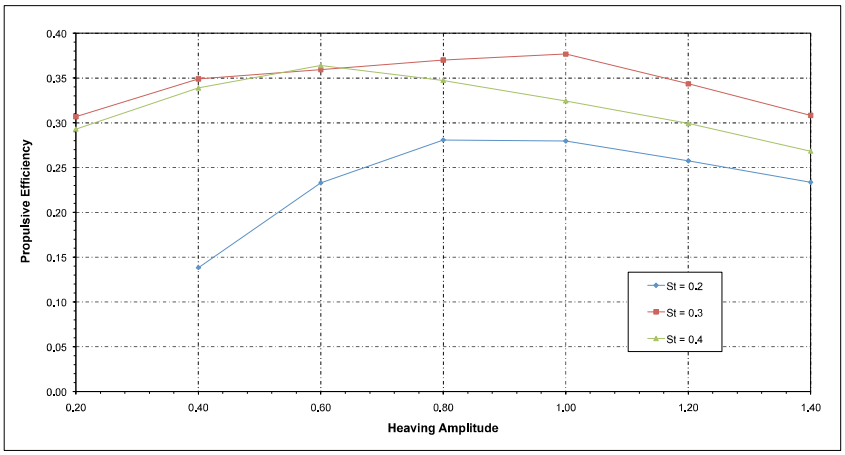

Figure 7.30: *Propulsive efficiency versus heaving amplitude for three different Strouhal number values. Flapping parameters:* $Re = 1100$, $\alpha_a = 20.0$.

7.4.4 Effect of Phase Angle

While a change in the heaving amplitude or flapping frequency has a predictable effect on the aerodynamic performance due to increased pressure differences, the effect of the phase angle is not very evident. In all the previous simulations, the phase angle value was set to $\varphi = 90$ degrees. Hereafter, we vary the phase angle between $80 < \varphi < 115$ degrees, and we fix the Strouhal number to $St = 0.25$, the heaving amplitude to $h_a = 0.5$ and the maximum pitching angle to $\alpha_a = 30$ degrees.

By varying the phase angle φ, the airfoil angle of attack is non-zero at the top and bottom positions. If the phase angle is greater than 90 degrees, at the lowest position of the heaving motion the airfoil will be pitched upwards, while if the phase angle is less than 90 degrees, at the same position the airfoil will be pitched downwards.

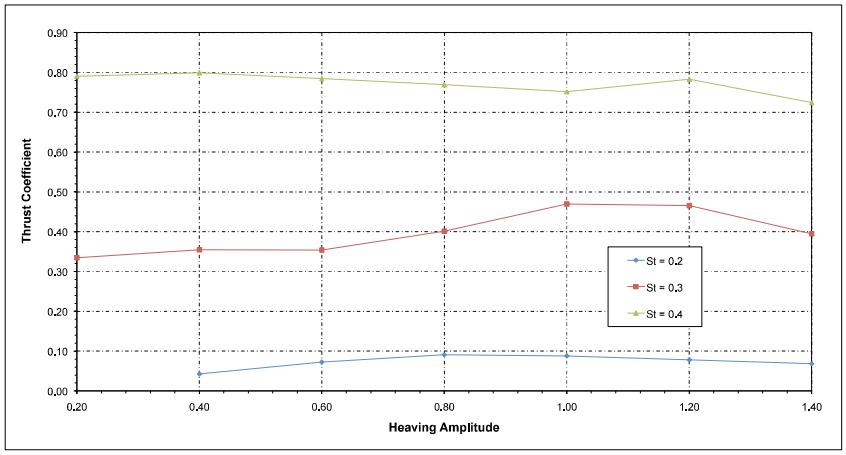

Figure 7.31: *Thrust coefficient versus heaving amplitude for three different Strouhal number values. Flapping parameters:* $Re = 1100$, $\alpha_a = 20.0$.

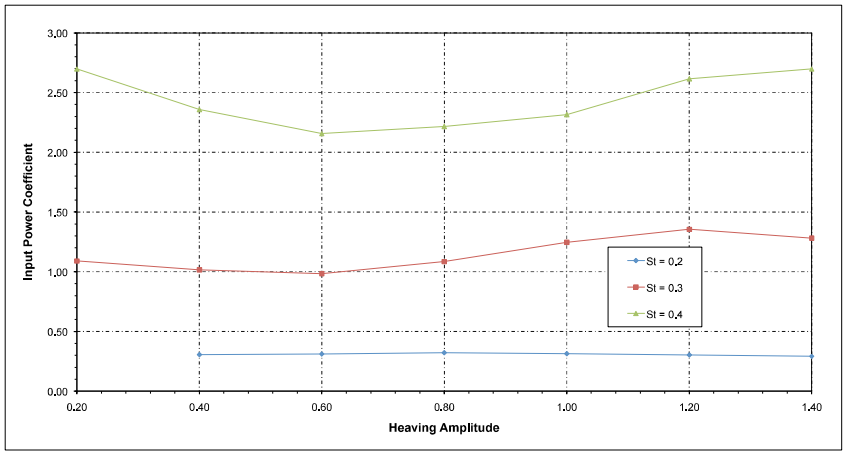

Figure 7.32: *Input power coefficient versus heaving amplitude for three different Strouhal number values. Flapping parameters:* $Re = 1100$, $\alpha_a = 20.0$.

In figure 7.33, the results for different cases simulated as per table 7.5 are plotted. In this figure, we can observe that for values of phase angle $\varphi > 90$ degrees the propulsive efficiency is enhanced reaching a maximum approximately at $\varphi = 100$ degrees and then it starts to decrease. For values greater than approximately 110 degrees, the propulsive efficiency is less than that generated at $\varphi = 90$ degrees. In this case, the best operating range is for phase angle values between $90 < \varphi < 110$ degrees.

In figure 7.34 we illustrate two different cases, one corresponding to a phase angle value equal to $\varphi = 100$ degrees and a second one corresponding to $\varphi = 90$ degrees, in this figure it can be observe that the phase angle has an effect on the LEV generation and shedding mechanism, clearly this influence the aerodynamic performance.

Case number	α_a (in degrees)	h_a	$\varphi(^\circ)$	St
2DF4-1	30.0	0.5	80.0	0.25
2DF4-2	30.0	0.5	85.0	0.25
2DF4-3	30.0	0.5	90.0	0.25
2DF4-4	30.0	0.5	95.0	0.25
2DF4-5	30.0	0.5	100.0	0.25
2DF4-6	30.0	0.5	105.0	0.25
2DF4-7	30.0	0.5	110.0	0.25
2DF4-8	30.0	0.5	115.0	0.25

Table 7.5: *Flapping parameters for the study of the effect of phase angle φ on the aerodynamic performance.*

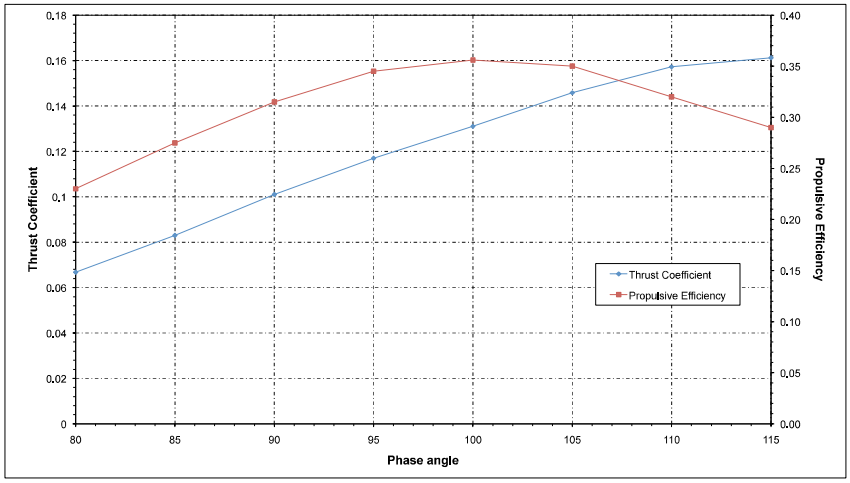

Figure 7.33: *Propulsive efficiency and average thrust coefficient in function of the phase angle φ. Flapping parameters: $Re = 1100$, $\alpha_a = 30.0$, $h_a = 0.5$, $St = 0.25$.*

7.4.5 Propulsive Efficiency, Thrust Coefficient and Input Power Coefficient Contour Maps

From the previous parametric studies, we can draw the following observations for optimal aerodynamic performance (in terms of propulsive efficiency, thrust generation and input power requirements):

- As for the pure heaving case, the best Strouhal number operating range is between $0.3 < St < 0.4$.
- The best operating pitching angle is between $20 < \alpha_a < 30$ degrees.
- Highest efficiency values with reasonable thrust coefficients are obtained for large amplitude values approximately between $0.8 < h_a < 1.2$.
- High propulsive efficiency accompanied by a high thrust coefficient of the order of one was obtained for $St = 0.4$.

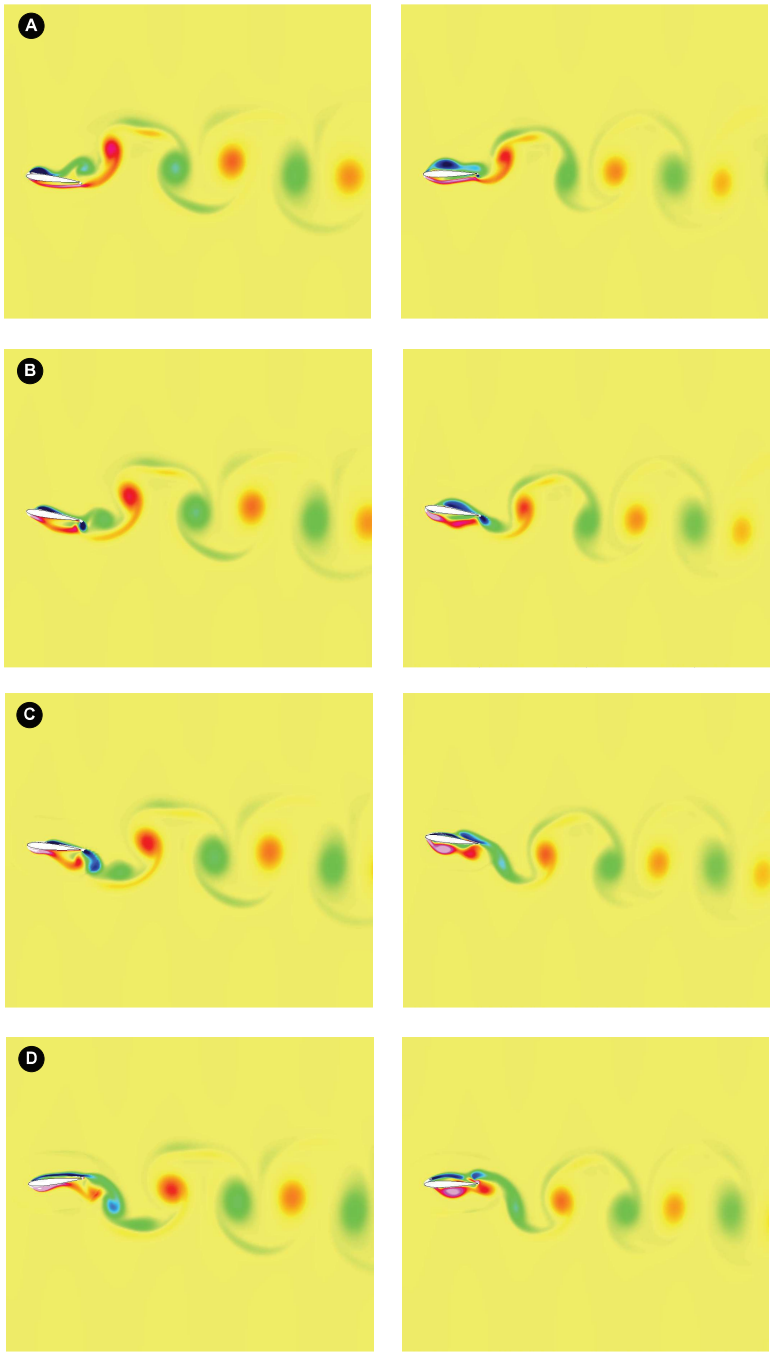

Figure 7.34: *Comparison of the vorticity field for two different flapping cases during upstroke. Left column: flapping airfoil with a phase angle equal to* $\varphi = 100°$*. Right column: flapping airfoil with a phase angle equal to* $\varphi = 90°$*. Flapping parameters:* $Re = 1100$*,* $St = 0.25$*,* $h_a = 0.25$*,* $\alpha_a = 10°$*. The sequence is shown for four instants during the upstroke motion, where: A) t = 8.0 B) t=8.35 C) t=8.70 D) t = 9.0*

- The maximum measured propulsive efficiency in the present set of numerical experiments was 64 percent.
- Phase angles in the range $90 < \varphi < 110$ give best propulsive efficiency without sacrificing thrust generation.

All the previous results are better summarized by plotting the solutions on contour maps for the propulsive efficiency, thrust coefficient and input power coefficient (nearly 80 simulation for each case presented). In figures 7.35, 7.36 and 7.37, we present the propulsive efficiency, thrust coefficient and input power coefficient contour maps for $St = 0.2$ as function of the heaving amplitude h_a and the maximum pitching angle α_a. In figure 7.35 we observe that at approximately $\alpha_a = 25$ degrees, the graph is divided in two parts. For values greater than $\alpha_a = 25$ degrees, little drag or no thrust is produced, while for values less than $\alpha_a = 25$ degrees little thrust is produce, this can be observed by looking at figure 7.36, where the thrust coefficient contour map is plotted. Overall, this case corresponds to a neutral wake.

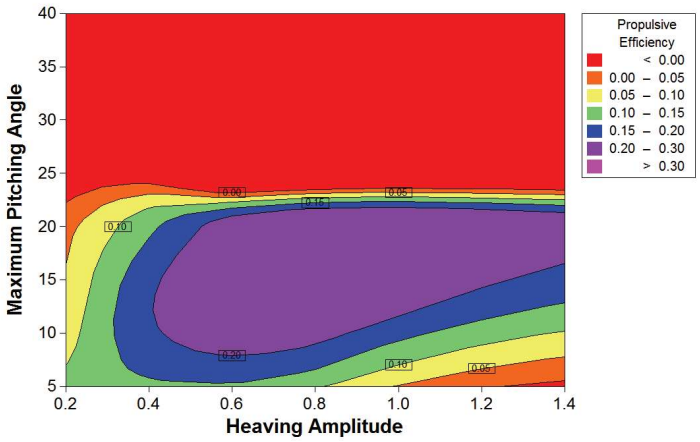

Figure 7.35: *Contour map of propulsive efficiency vs. maximum pitching angle and heaving amplitude. Flapping parameters:* $Re = 1100$, $St = 0.2$

In figures 7.38, 7.39 and 7.40, we present the propulsive efficiency, thrust coefficient and input power coefficient contour maps for $St = 0.3$ as function of the heaving amplitude h_a and the maximum pitching angle α_a. By looking at figure 7.38 and comparing with figure 7.35, the efficiency rapidly increases from relatively low values to relatively high values as the Strouhal number is increased. In this figure, the maximum efficiency values are achieved at heaving amplitudes between $0.8 < h_a < 1.4$ and maximum pitching angles between $25 < \alpha_a < 35$ degrees. In figure 7.40, we observe that the input power coefficient is very high for low amplitudes and maximum pitching angle α_a above 15 degrees. This behavior is expected to occur at low amplitudes, due to the fact that a lot of vorticity is produced near the leading edge and is converted into high input power requirements. By inspecting figure 7.39, we notice that this is a thrust producing case in almost all the range of heaving amplitudes and maximum pitching angles simulated.

In figures 7.41, 7.42 and 7.43, the propulsive efficiency, thrust coefficient and input power coefficient contour maps for $St = 0.4$ as function of the heaving amplitude h_a and the maximum

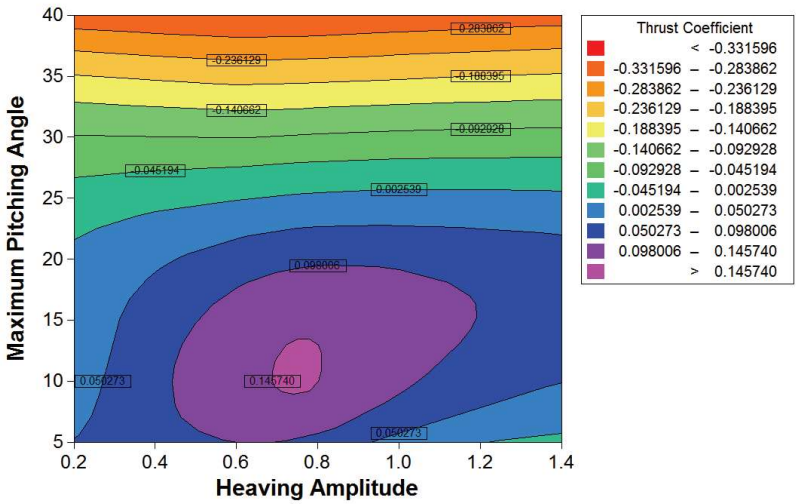

Figure 7.36: *Contour map of thrust coefficient vs. maximum pitching angle and heaving amplitude. Flapping parameters:* $Re = 1100$, $St = 0.2$.

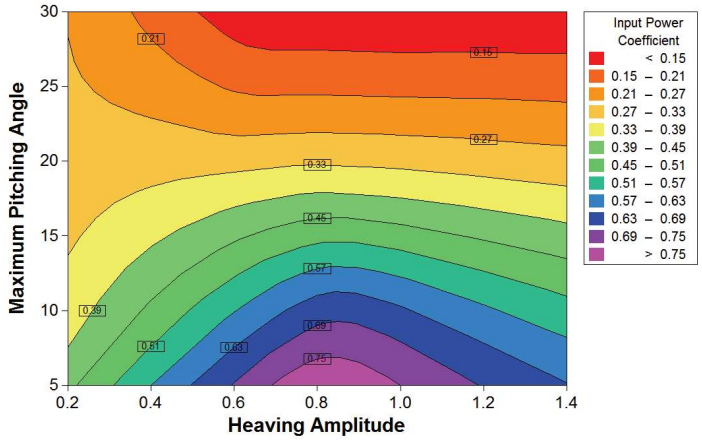

Figure 7.37: *Contour map of input power coefficient vs. maximum pitching angle and heaving amplitude. Flapping parameters:* $Re = 1100$, $St = 0.2$.

pitching angle α_a are plotted. From figure 7.41, we observe that the maximum efficiency values are achieved at high heaving amplitudes between $1.0 < h_a < 1.4$ and maximum pitching angles between $25 < \alpha_a < 40$ degrees. Looking at figure 7.42, we can also identify two *"high thrust"* areas, one corresponding to *"low efficiency"* (for values of heaving amplitude between $0.4 < h_a < 0.6$) and the second one corresponding to *"high efficiency"* (for values of heaving amplitude between $1.0 < h_a < 1.4$). As for the previous case ($St = 0.3$), we observe high input power coefficient values at low amplitudes (see figure 7.43). By examining figure 7.42, it can be inferred that this is a thrust producing case in almost all the range of heaving amplitudes and maximum pitching angles simulated.

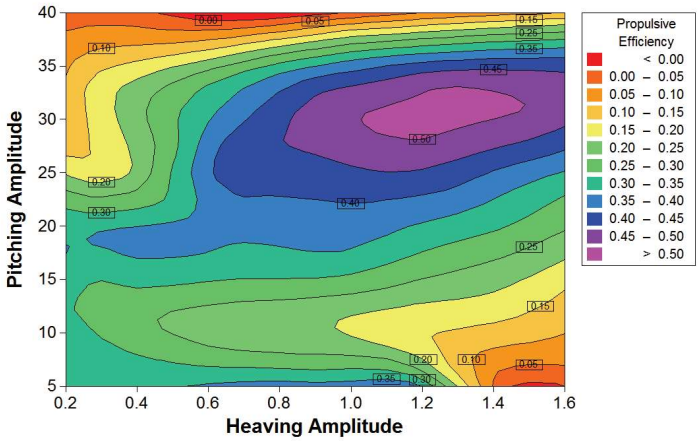

Figure 7.38: *Contour map of propulsive efficiency vs. maximum pitching angle and heaving amplitude. Flapping parameters:* $Re = 1100$, $St = 0.3$

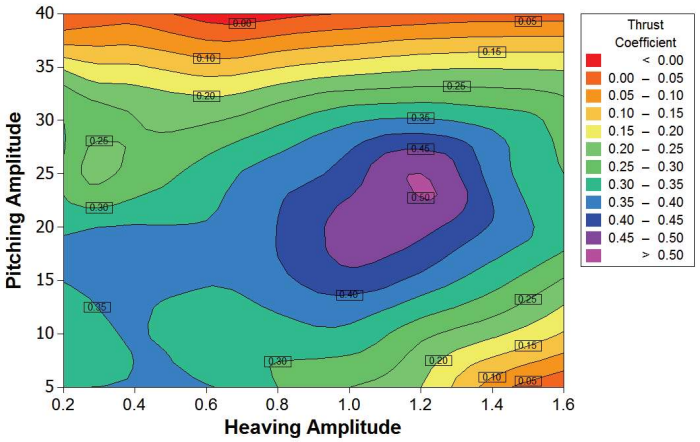

Figure 7.39: *Contour map of thrust coefficient vs. maximum pitching angle and heaving amplitude. Flapping parameters:* $Re = 1100$, $St = 0.3$.

In figures 7.44 and 7.45, we present the vorticity field for several flapping cases. In figure 7.44, where $St = 0.2$, we can observe that the wake topology does not shows the typical mushroom-shaped structure for typical thrust production regimes; in fact, the cases shown produce drag or little thrust. It can be also observed that as we increase the maximum pitching angle, the strength of the LEV is lowered. In figure 7.45 (corresponding to $St = 0.4$), we can now identify the typical mushroom structure for thrust producing wakes; as in the previous case, as we increase the maximum pitching angle the strength of the LEV is weakened and this translates into lower input power requirements.

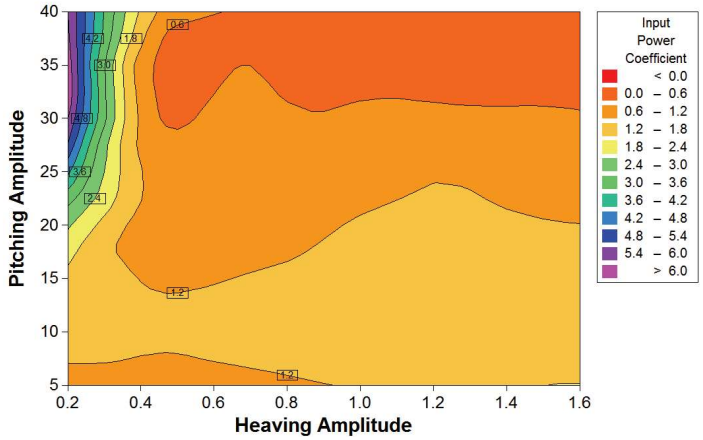

Figure 7.40: *Contour map of input power coefficient vs. maximum pitching angle and heaving amplitude. Flapping parameters:* $Re = 1100$, $St = 0.3$.

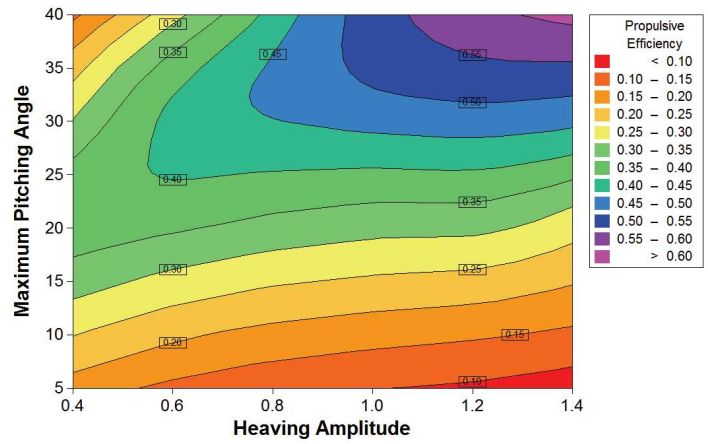

Figure 7.41: *Contour map of propulsive efficiency vs. maximum pitching angle and heaving amplitude. Flapping parameters:* $Re = 1100$, $St = 0.4$

7.5 Heaving Airfoil Vs. Flapping Airfoil

In the previous sections, we studied heaving and flapping airfoils aerodynamic performance. From the results obtained, it is evident that flapping airfoils provide in general better aerodynamic performance than purely heaving airfoils. In figures 7.46, 7.47 and 7.48, we compare the aerodynamic performance for a heaving airfoil and a flapping airfoil. The cases are compared for a Strouhal number value equal to $St = 0.3$.

As it can be seen in figure 7.46, for heaving amplitudes less than 0.2, the pure heaving motion provides better propulsive efficiency than the flapping motion. On the other hand, for values higher than 0.2 the flapping motion gives the best propulsive efficiency, with its value increasing very fast with the heaving amplitude. This behavior is expected to occur for flapping airfoils

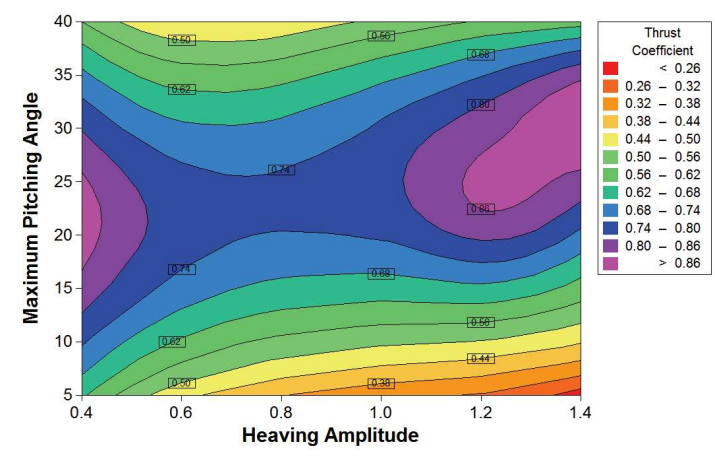

Figure 7.42: *Contour map of thrust coefficient vs. maximum pitching angle and heaving amplitude. Flapping parameters:* $Re = 1100$, $St = 0.4$.

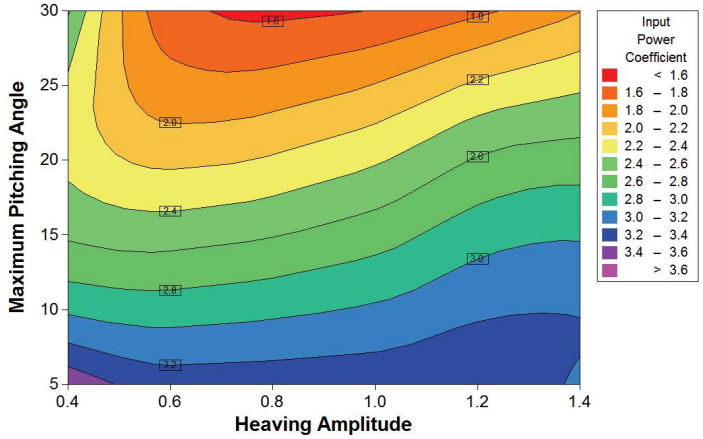

Figure 7.43: *Contour map of input power coefficient vs. maximum pitching angle and heaving amplitude. Flapping parameters:* $Re = 1100$, $St = 0.4$.

heaving with low heaving amplitudes, due to the fact that vorticity is produced near the leading edge and converted into high input power coefficients, as seen in figure 7.48. Commenting on the thrust coefficient (figure 7.47), we can observe that for both kinds of kinematics the maximum thrust coefficient is almost identical when operating at high efficiency values, but with the difference that for the flapping case, the high thrust coefficient values are maintained over a wider range of heaving amplitudes.

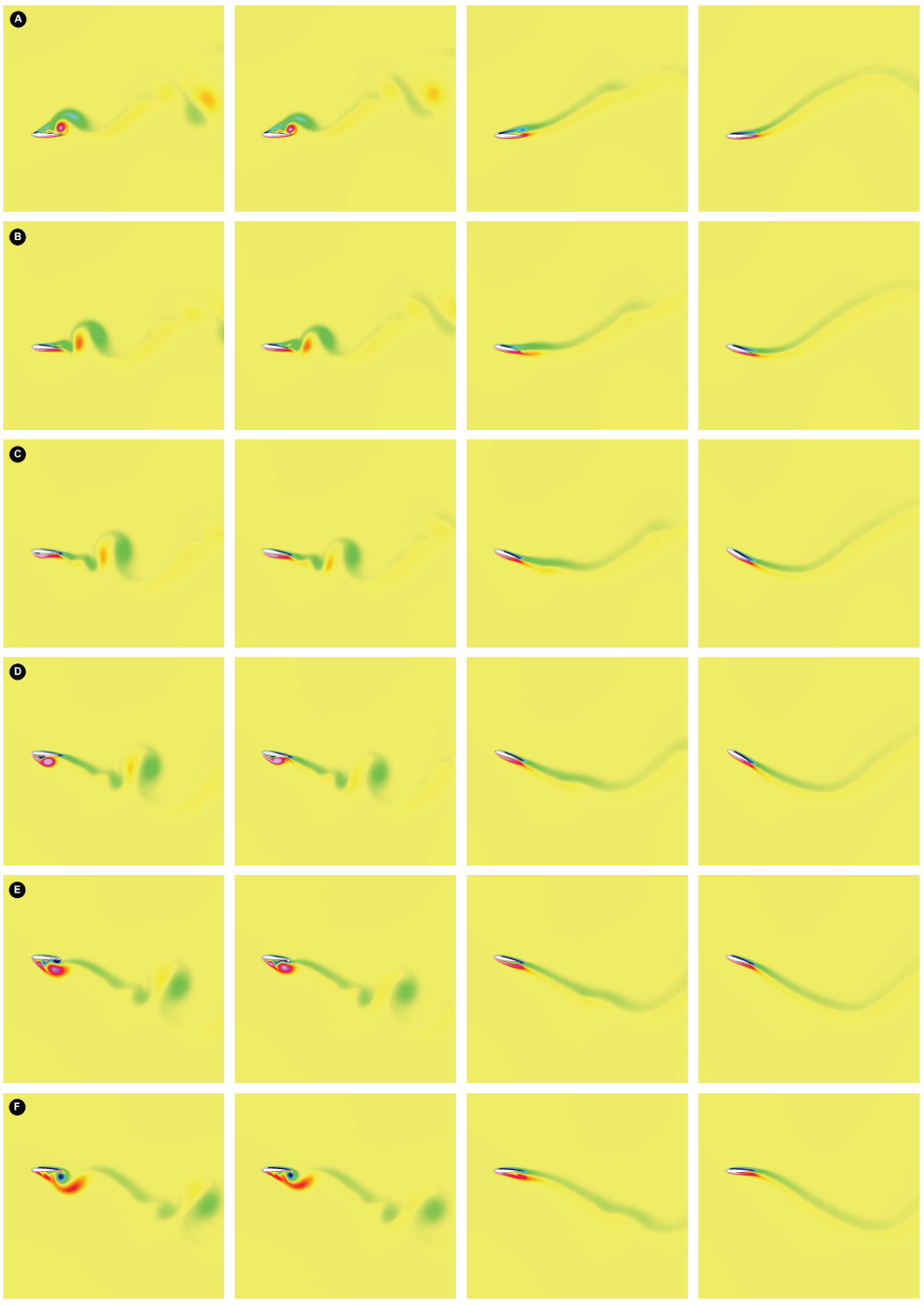

Figure 7.44: *Comparison of the vorticity field for four different flapping cases during upstroke. First column:* $Re = 1100$, $St = 0.2$, $h_a = 1.0$, $\alpha_a = 5°$, $\varphi = 90°$. *Second column:* $Re = 1100$, $St = 0.2$, $h_a = 1.0$, $\alpha_a = 10°$, $\varphi = 90°$. *Third column:* $Re = 1100$, $St = 0.2$, $h_a = 1.0$, $\alpha_a = 20°$, $\varphi = 90°$. *Fourth column:* $Re = 1100$, $St = 0.2$, $h_a = 1.0$, $\alpha_a = 30°$, $\varphi = 90°$. *The sequence is shown for six instants during the upstroke motion, where: A)* $t = 30.0$ *B)* $t = 31.0$ *C)* $t = 32.0$ *D)* $t = 33.0$ *E)* $t = 34.0$ *F)* $t = 35.0$.

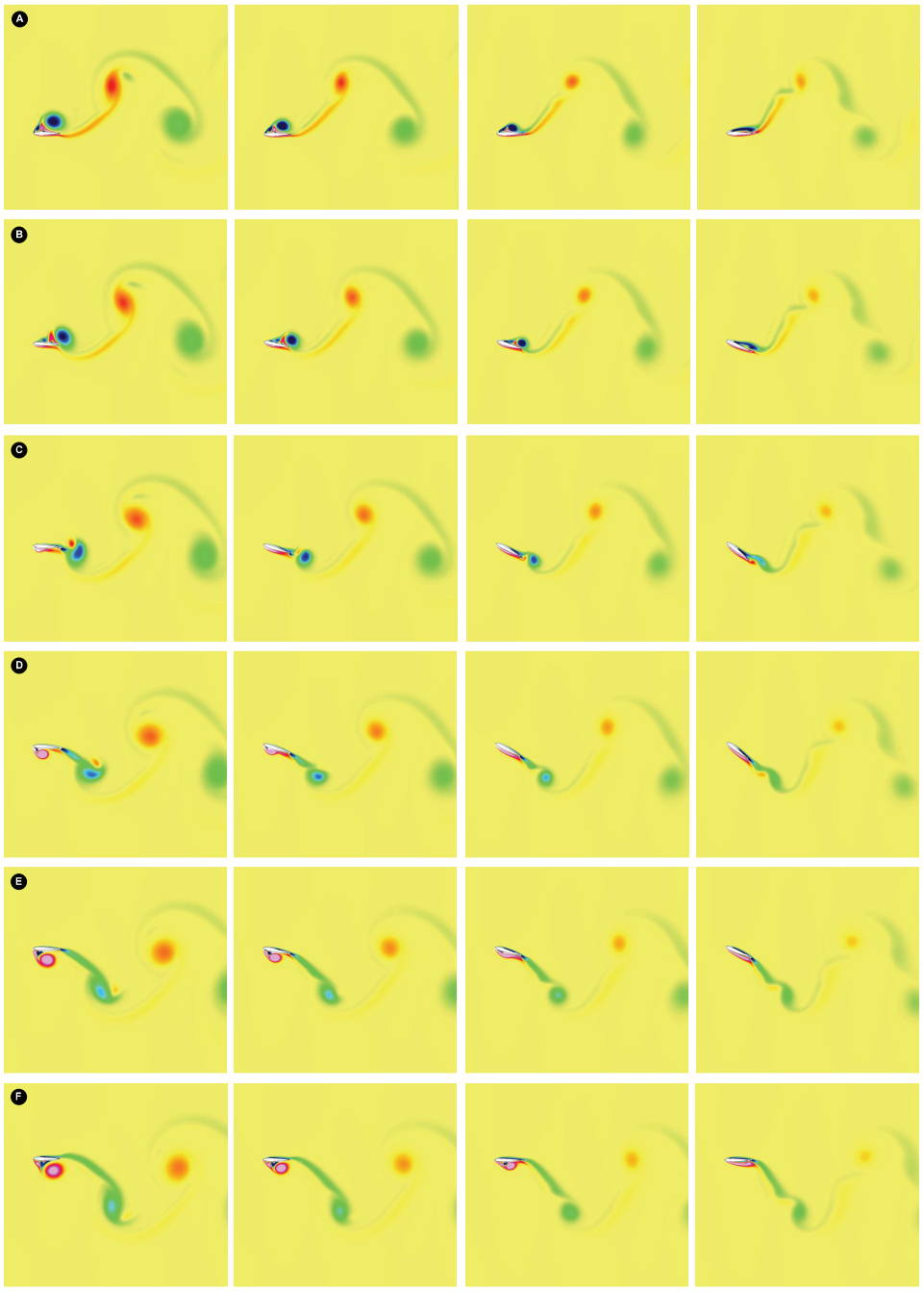

Figure 7.45: *Comparison of the vorticity field for four different flapping cases during upstroke. First column:* $Re = 1100$, $St = 0.4$, $h_a = 1.0$, $\alpha_a = 5°$, $\varphi = 90°$. *Second column:* $Re = 1100$, $St = 0.4$, $h_a = 1.0$, $\alpha_a = 20°$, $\varphi = 90°$. *Third column:* $Re = 1100$, $St = 0.4$, $h_a = 1.0$, $\alpha_a = 30°$, $\varphi = 90°$. *Fourth column:* $Re = 1100$, $St = 0.4$, $h_a = 1.0$, $\alpha_a = 40°$, $\varphi = 90°$. *The sequence is shown for six instants during the upstroke motion, where: A)* $t = 20.0$ *B)* $t = 20.5$ *C)* $t = 21.0$ *D)* $t = 21.5$ *E)* $t = 22.0$ *F)* $t = 22.5$.

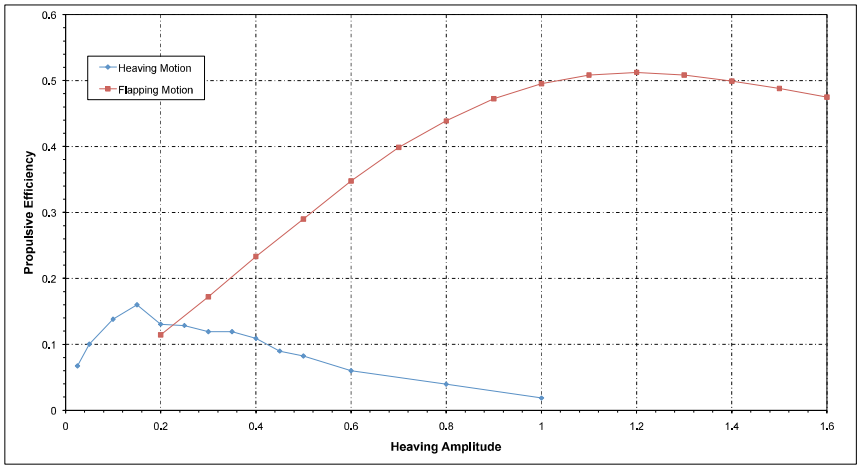

Figure 7.46: *Heaving and flapping motions propulsive efficiency comparison. Flapping parameters:* $Re = 1100$, $St = 0.3$, $\alpha_a = 30.0$.

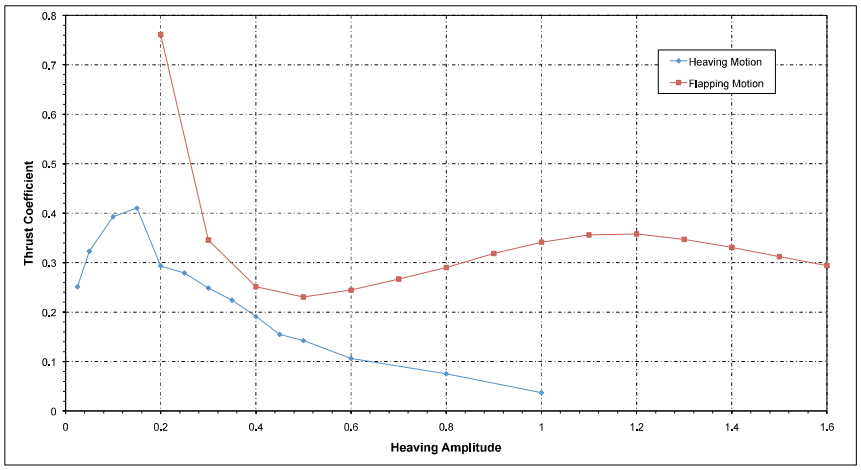

Figure 7.47: *Heaving and flapping motions thrust coefficient comparison. Flapping parameters:* $Re = 1100$, $St = 0.3$, $\alpha_a = 30.0$.

7.6 Effect of Flexibility on the Aerodynamic Performance

Despite the growing interest in modeling and understanding the physics of flexible flapping wings, this field of study remains largely unexplored. In this section, we briefly investigate the effect of chord-wise flexure amplitude on the aerodynamic performance of a NACA 0012 airfoil undergoing pure heaving motion. Here we impose the airfoil deformation as follows

$$y = \frac{h_{flex}}{c} x^2 cos\left(2\pi f_{flex} t + \varphi\right), \tag{7.3}$$

as proposed by Miao and Ho [124]. In eq. 7.3, h_{flex} is the flexure amplitude, c the airfoil chord, x are the airfoil horizontal coordinates, y are the airfoil new vertical coordinates, f_{flex} is the

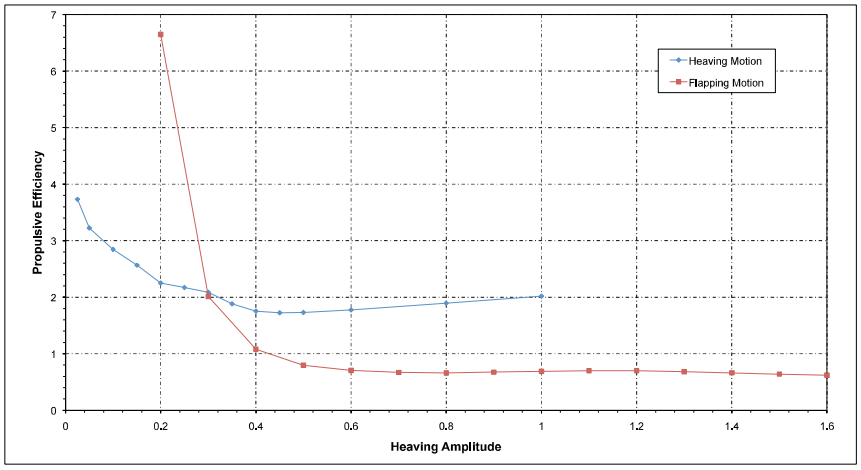

Figure 7.48: *Heaving and flapping motions input power coefficient comparison. Flapping parameters:* $Re = 1100$, $St = 0.3$, $\alpha_a = 30.0$.

flexure frequency (which is assumed to be the same as the heaving frequency) and φ is the phase angle. In order to investigate the effect of the flexure amplitude on the aerodynamic performance of heaving wings, we consider six different flexure amplitudes h_{flex}, as shown in table 7.6. The value $h_{flex} = 0.0$ corresponds to the rigid airfoil case.

Case number	h_{flex}	$\varphi(^\circ)$	h_a	St
2DF5-1	0.1	90.0	0.25	0.3
2DF5-2	0.2	90.0	0.25	0.3
2DF5-3	0.3	90.0	0.25	0.3
2DF5-4	0.4	90.0	0.25	0.3
2DF5-5	0.5	90.0	0.25	0.3
2DF5-6	0.6	90.0	0.25	0.3

Table 7.6: *Flapping parameters for the study of the flexible heaving airfoil.*

Figure 7.49, shows the variation of propulsive efficiency and average thrust coefficient with respect to the flexure amplitude. Comparing the results with the rigid body case, an enhancement in the propulsive efficiency and thrust coefficient is observed, until a value of $h_{flex} = 0.4$ from which point on the propulsive efficiency starts to decrease. This observation is in agreement with the results of Heatcote and Gursul [67, 68], where they found that adding a degree of flexibility increase both thrust and propulsive efficiency. To explain this improvement in the aerodynamics performance, let us suppose that the airfoil deformation can be approximated as an imposed pitch angle, and as studied in previous section; if we increase the maximum pitching angle during flapping motion, the aerodynamic performance is enhanced. In figure 7.50 we illustrate a deforming case, where we set the maximum flexure amplitude to $h_{flex} = 0.3$, the heaving amplitude to $h_a = 0.25$ and the Strouhal number to $St = 0.3$. For purposes of comparison, we also plot in figure 7.51 the equivalent rigid airfoil case. In figure 7.50, it can be observed that the airfoil deformation helps to convect the LEV more smoothly from the leading edge to the trailing edge; furthermore, the

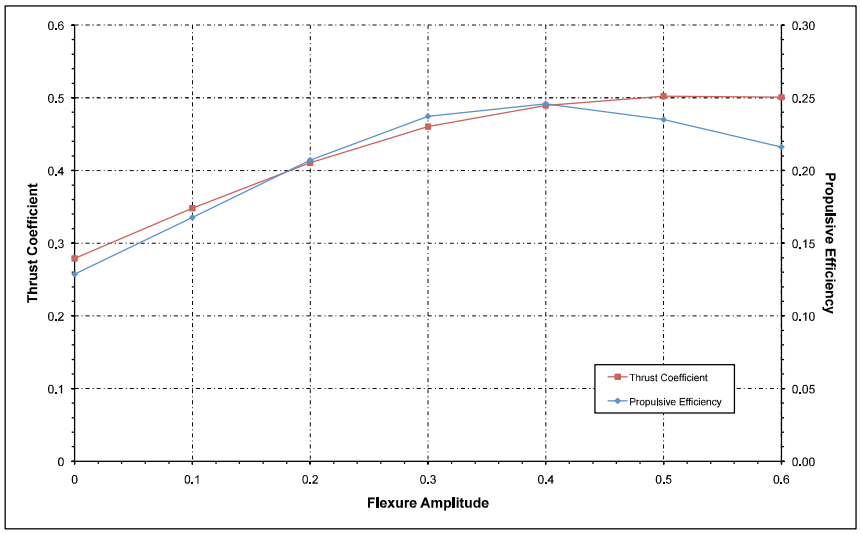

Figure 7.49: *Comparison of propulsive efficiency and average thrust coefficient versus flexure amplitude. Flapping parameters:* $Re = 1100$, $St = 0.3$, $h_a = 0.25$.

strength of the LEV is less than in the equivalent rigid case.

7.7 Effect of Airfoil Cambering on the Aerodynamic Performance

The effect of airfoil cambering on the aerodynamic performance of heaving or flapping airfoils still remains virtually unexplored, even though it is crucial on lift generation. Bird wings actually have camber due to the need of lift generation. The fact that this area have not been sufficiently studied, is related to the fact that most researchers have used symmetrical airfoils in their investigations [62, 89, 94, 96, 108, 140, 151, 197, 207, 216], as they are chiefly interested on thrust generation and propulsion efficiency.

In this section, we conduct a parametric study in order to assess the effect of airfoil cambering on the aerodynamic performance (in particular the lift coefficient c_l) of heaving airfoils. The airfoils used for this study are listed in table 7.7; basically, we used a standard NACA four digits series airfoil, where we simply change the maximum airfoil cambering and its position. Additionally, we also use the high lift low Reynolds number Selig S1223 airfoil. This latter airfoil was chosen because of its similarities to the Seagull and Merganser wings cross-section, as suggested by Liu *et al.* [114]. In table 7.8, the parameters governing the heaving motion are shown. Here, two heaving amplitudes are used, one corresponding to high heaving frequencies and one corresponding to low heaving frequency.

The summary of results is presented in tabular form in tables 7.9 and 7.10, where $\overline{c_t}$ is the average thrust coefficient, $\overline{c_P}$ is the average input power coefficient, $\overline{c_l}$ is the average lift coefficient, η is the propulsive efficiency and $\hat{c}_l$ is the maximum lift coefficient. Inspecting table 7.9 and using the results of the NACA 0012 airfoil as a reference, we observe that the values of $\overline{c_t}$, $\overline{c_P}$, η and $\hat{c}_l$ do not change much as the maximum airfoil cambering and its position are modified; conversely, looking at the values of $\overline{c_l}$, we observe that its values increase as we change the maximum airfoil

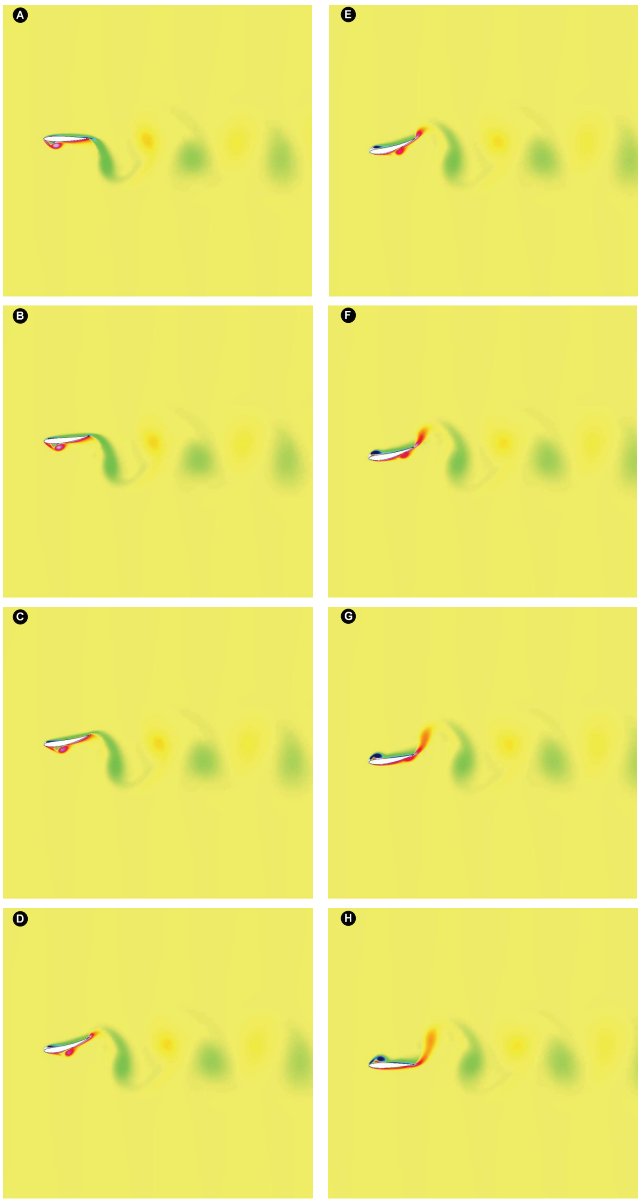

Figure 7.50: *Vorticity field for the flexible airfoil study. The sequence is shown for eight instants during the downstroke motion, where: A) t = 8.33 B) t= 8.45 C) t= 8.55 D) t = 8.70 E) t = 8.80 F) t=8.90 G) t=9.0 H) t=9.16. Flapping parameters:* $Re = 1100$, $h_{flex} = 0.3$, $h_a = 0.25$, $St = 0.3$.

cambering and its position, in fact, we are now producing a positive average lift coefficient $\overline{c_l}$.

In table 7.10, the results for a case similar to the previous one but with a heaving amplitude equal to $h_a = 0.3$ and a heaving frequency equal to $f_h = 0.666667$ are presented. In this table, the same observations as for the previous case hold. Looking closely at the aerodynamic quantities for the S1223 airfoil, we notice that the aerodynamic performance of this airfoil is not close to that of the other airfoils; nevertheless, it still produces thrust and lift.

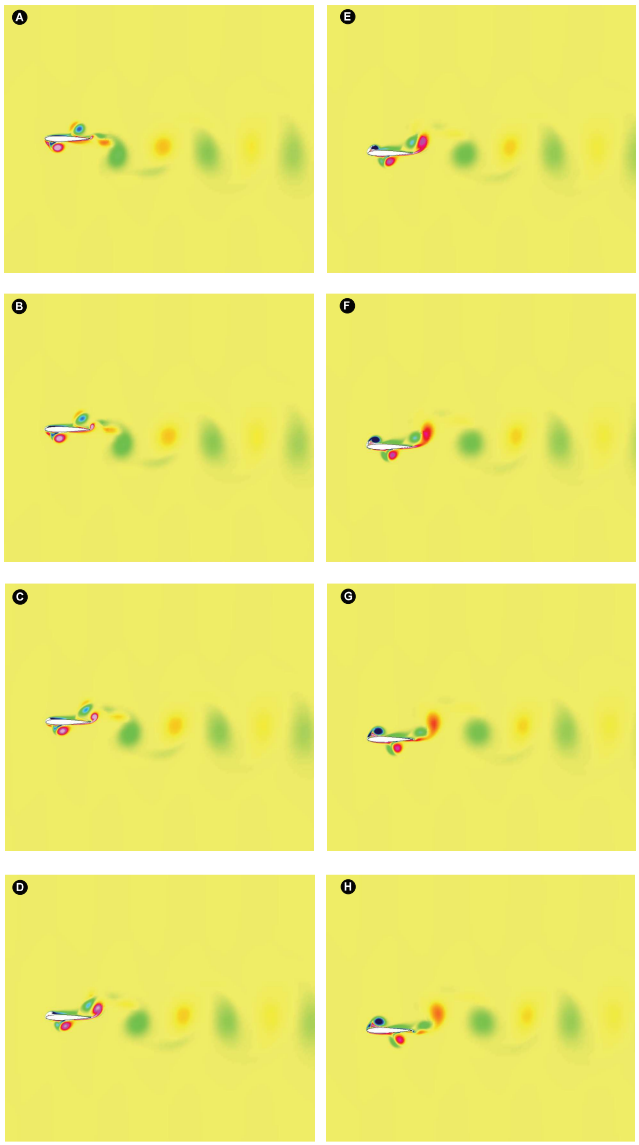

Figure 7.51: *Vorticity field for the flexible airfoil study (rigid airfoil case). The sequence is shown for eight instants during the downstroke motion, where: A) t = 8.33 B) t= 8.45 C) t= 8.55 D) t = 8.70 E) t = 8.80 F) t=8.90 G) t=9.0 H) t=9.16. Flapping parameters:* $Re = 1100$, $h_{flex} = 0.0$, $h_a = 0.25$, $St = 0.3$.

From the previous results and having in mind that if we are interested in flying we need to produce lift, the use of cambering in flapping flight is favorable and it does not cause detriment in the aerodynamic performance. In figure 7.52, a comparison of the vorticity field for a NACA 0012 and a Selig S1223 airfoil is presented. Notice that the vorticity field for the S1223 airfoil is no more symmetric, hence the strength and shedding of the vortices during the upstroke and downstroke are different. The sequence in figure 7.52 is shown for four instants during the upstroke motion. For completeness, in figure 7.53 we present the vorticity field for a NACA 2212 airfoil

7.7. EFFECT OF AIRFOIL CAMBERING ON THE AERODYNAMIC PERFORMANCE

Airfoil Type
NACA 0012
NACA 2212
NACA 2412
NACA 4412
NACA 2612
NACA 4612
NACA 6612
Selig S1223

Table 7.7: *Airfoils used for the study of cambering effect on the aerodynamic performance of heaving airfoils.*

Case number	h_a	f_h	$\varphi(^\circ)$	St
2DF5-1	0.1	1.5	90.0	0.4
2DF5-2	0.3	0.5	90.0	0.4

Table 7.8: *Heaving parameters for the study of airfoil cambering effect on the aerodynamic performance.*

Airfoil type	$\overline{c_t}$	$\overline{c_P}$	η	$\overline{c_l}$	$\hat{c_l}$
NACA 0012	0.8515	7.5748	0.1124	0.009397	28.1761
NACA 2212	0.9326	7.6910	0.1212	0.028386	27.0256
NACA 2412	0.9329	7.7209	0.1208	0.1120	27.1245
NACA 4412	0.9080	7.6433	0.1188	0.4465	27.4484
NACA 2612	0.9286	7.7304	0.1201	0.2475	28.5417
NACA 4612	0.8920	7.6356	0.1168	0.7074	28.8189
NACA 6612	0.8664	7.5440	0.1148	1.1194	28.2583
Selig S1223	0.7944	7.2373	0.1097	1.4181	29.5885

Table 7.9: *Comparison of the aerodynamic performance of eight different airfoils for the study of cambering effect on the aerodynamic behavior. Flapping parameters:* $Re = 1100$, $St = 0.4$, $h_a = 0.1$, $f_h = 2.0$

Airfoil type	$\overline{c_t}$	$\overline{c_P}$	η	$\overline{c_l}$	$\hat{c_l}$
NACA 0012	0.8292	5.3332	0.1554	0.0144	11.3097
NACA 2212	0.8244	5.3221	0.1549	0.2279	11.0896
NACA 2412	0.8486	5.3313	0.1591	0.1074	10.4898
NACA 4412	0.8035	5.2321	0.1535	0.1584	10.7599
NACA 2612	0.8340	5.3293	0.1565	0.3194	11.4170
NACA 4612	0.8067	5.2851	0.1526	0.3963	11.5470
NACA 6612	0.7627	5.1025	0.1494	0.4675	12.7073
Selig S1223	0.4284	4.4070	0.0972	0.2658	11.5889

Table 7.10: *Comparison of the aerodynamic performance of eight different airfoils for the study of cambering effect on the aerodynamic behavior. Flapping parameters:* $Re = 1100$, $St = 0.4$, $h_a = 0.3$, $f_h = 2.0$

and a NACA 4612 airfoil under the same previous flapping conditions. Notice in figure 7.53 that as we added camber, the vorticity shedding is no longer symmetric, also, by examining the wake we can observe that the added airfoil cambering induce a small upward deflection on the wake.

7.8 Summary

In this chapter, we studied the dependency of the wake structure and aerodynamic performance on the flapping and geometric parameters such as flapping frequency, flapping amplitude, airfoil geometry and airfoil chord-wise flexibility (among others), for airfoils undergoing pure heaving motion or flapping motion.

It was found that the Strouhal number (based on the heaving amplitude h_a) seems to be enough for wake signature characterization, but is not sufficient insofar as maximum efficiency is concerned. Both heaving amplitude h_a and heaving frequency f_h (hence the Strouhal number St and the reduced frequency k), should be adjusted separately.

All the qualitative and quantitative results agree with the hypothesis that : *"flying and swimming animals cruise at a Strouhal number tuned for high power efficiency"* [182]. The enhanced efficiency range was found to be between Strouhal number values corresponding to $0.2 < St < 0.4$, which agrees with the observations of Taylor *et al.* [182], Triantafyllou *et al.* [193] and Nudds *et al.* [136].

It was also observed different behaviors on the aerodynamic performance for high flapping frequencies (low heaving amplitudes) and low flapping frequencies (high heaving amplitudes). Firstly, at high flapping frequencies f the LEV does not have sufficient time to grow, whereas at low flapping frequencies f the vortex can become a sizable fraction of the airfoil chord before separating. Thus the impact of the vortex on the pressure at the nose of the airfoil is dependent on the flapping frequency. Secondly, once the vortex separates it is convected downstream over the surface of the airfoil. Due to the low pressure in the vortex core this has the effect of maintaining thrust while the vortex is upstream of the airfoil maximum thickness point (where the airfoil surface is tilted upstream and the vortex low pressure creates an upstream suction force). Once passing this point, the airfoil surface is tilted downstream and the vortex contributes to drag rather than thrust. At high flapping frequencies, the vortex cannot be convected far downstream before the motion cycle creates another leading edge on the opposite side of the airfoil, so the impact is lessened. At low flapping frequencies f however, the vortex travels far downstream over the airfoil surface causing drag for a larger portion of the flapping cycle and therefore lowering the propulsive efficiency.

For flapping motion, where the orientation of the airfoil surface is controlled by the relative amplitudes and phases of the motion, the LEV may create positive thrust for much longer portions of the flapping cycle and thus contribute towards the propulsive efficiency. Also, for flapping motion the average input power coefficient is less than the average input power coefficient for the heaving motion cases, resulting in an improved propulsive efficiency. It was also observed that the best propulsive efficiencies were obtained for high heaving amplitudes (between $0.8 < h_a < 1.2$), in contrast to the heaving motion were the propulsive efficiency is degraded as the heaving amplitude is increased above a value of $h_a = 0.2$.

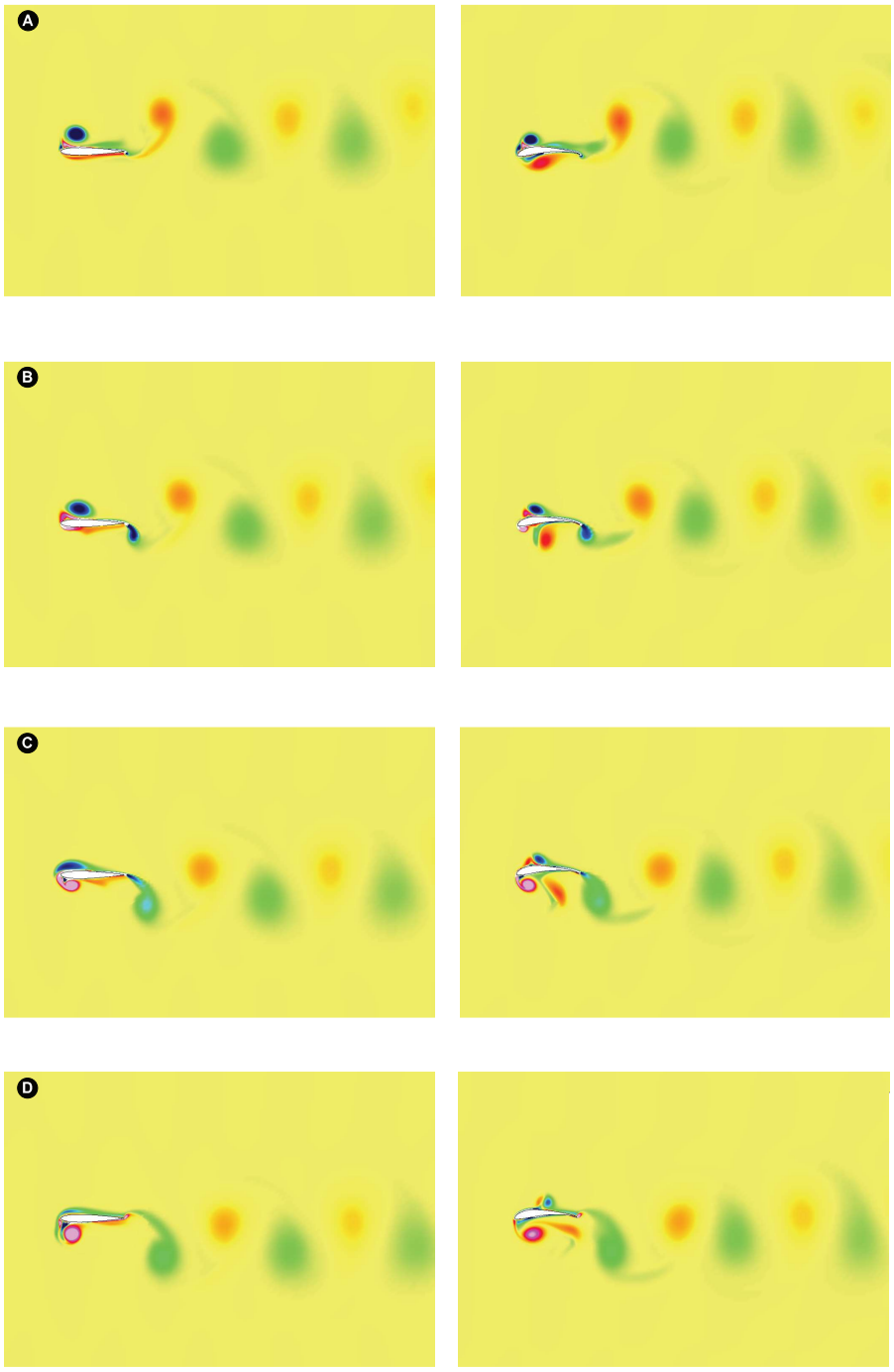

Figure 7.52: *Comparison of the vorticity field for two different airfoils. Left column: NACA 0012 airfoil. Right column: Selig S1223 airfoil. Flapping parameters:* $Re = 1100$, $St = 0.4$, $h_a = 0.3$. *The sequence is shown for four instants during the upstroke motion, where: A)* $t = 9.0$ *B)* t=9.25 *C)* t=9.50 *D)* $t = 9.75$.

In this chapter the effect of chord-wise flexibility on the aerodynamic performance of heaving airfoils was also explored. Thrust-indicative wake topologies were observed for the whole range of flexure amplitudes tested. The results also shown that the propulsive efficiency is enhanced for values of $h_{flex} < 0.4$. This observation is in agreement with the results of Heatcote and Gursul [67, 68], where they found that adding a degree of flexibility increases both thrust and propulsive efficiency. They also suggested that birds, bats and insects may benefit aerodynamically from the flexibility of their wings.

Finally, the effect of airfoil cambering on the aerodynamic performance was assessed. It was found that this geometric parameter has a strong influence on the lift coefficient, while it has a small impact on the thrust coefficient and propulsive efficiency. Among all the asymmetric airfoils used, the NACA 6612 airfoil provided the best propulsive efficiency and average lift coefficient, which along with the thrust generation are the crucial factors if we are interested in flapping flight. The S1223 airfoil, which resembles the cross-section of the Seagull and Merganser wings (as observed by Liu *et al.* [114]), provided at high heaving frequencies the biggest average lift coefficient and very similar average thrust coefficient and propulsive efficiency values when compared to the other airfoils. On the other hand, at low heaving frequencies, the aerodynamic performance of the S1223 airfoil was deteriorated in comparison to the other airfoils, while still producing thrust and positive average lift.

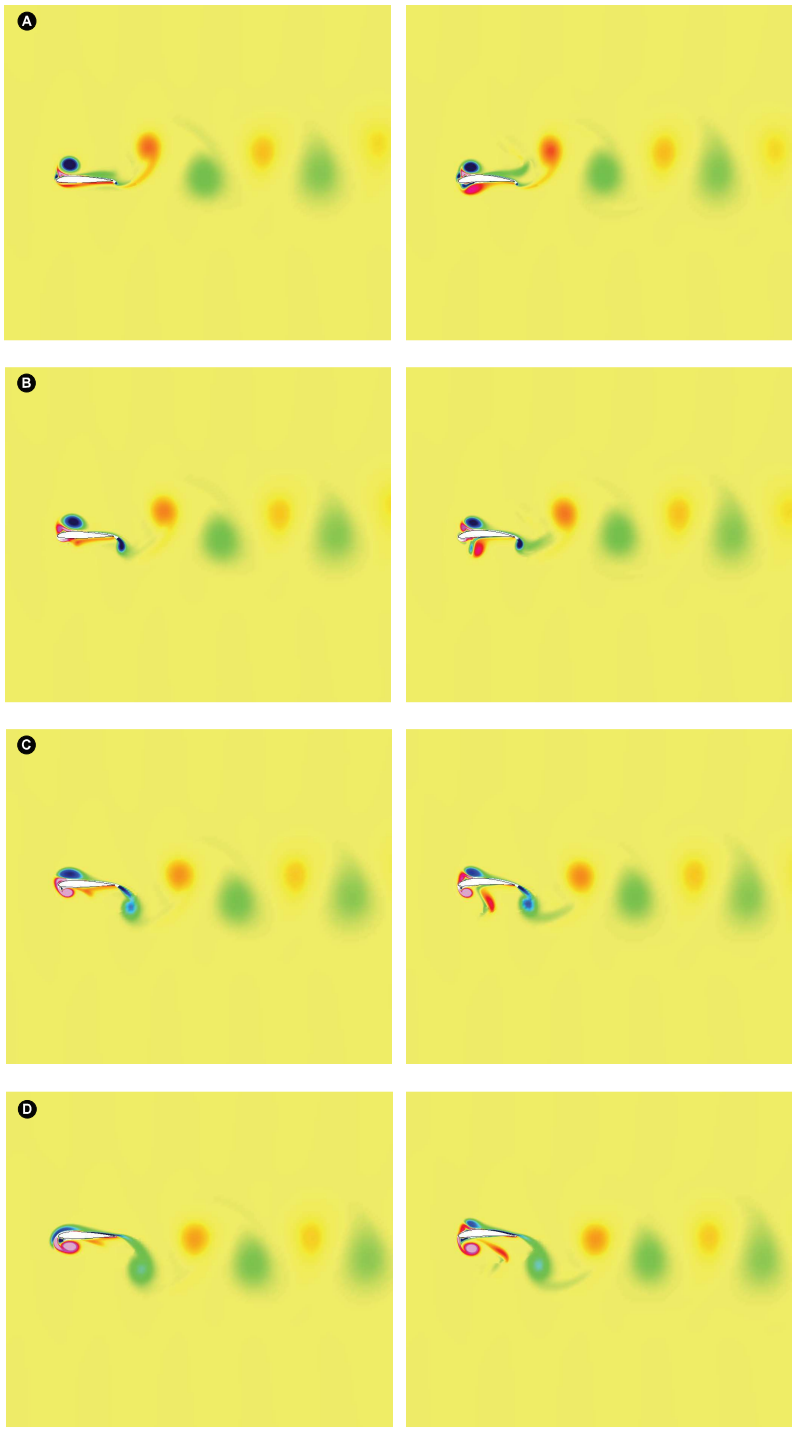

Figure 7.53: *Comparison of the vorticity field for two different airfoils. Left column: NACA 2212 airfoil. Right column: NACA 4612. Flapping parameters:* $Re = 1100$, $St = 0.4$, $h_a = 0.3$. *The sequence is shown for four instants during the upstroke motion, where: A)* $t = 9.0$ *B)* t*=9.25 C)* t*=9.50 D)* $t = 9.75$.